Fakultät für Medizin

INVESTIGATION OF ACUTE RADIATION EFFECTS AFTER MINIBEAM IRRADIATION WITH PROTONS IN MURINE SKIN

Esther Maria Zahnbrecher

Vollständiger Abdruck der von der Fakultät für Medizin der Technischen Universität München zur Erlangung des akademischen Grades eines Doktors der Medizin (Dr. med.) genehmigten Dissertation.

Vorsitzender: Prof. Dr. Jürgen Schlegel

Prüfende/-r der Dissertation:

1. apl. Prof. Dr. Thomas E. Schmid

2. apl. Prof. Dr. Bernadette Eberlein

Die Dissertation wurde am 21.10.2019 bei der Technischen Universität München eingereicht und durch die Fakultät für Medizin am 12.05.2020 angenommen.

Abstract

Purpose

In Radiation Oncology, the maximum dose which can be delivered to a certain tumour is often limited by the radiation-induced damage in normal tissue surrounding the actual tumour. Minibeam Radiation Therapy with Protons (pMBRT) aims to minimise normal tissue damage, especially in the entrance channel. Due to beam widening with increasing track length, it results in a homogeneous dose distribution in the tumour area, which permits tumour control as in conventional proton therapy. In this study, the effect of partially widened proton minibeams was investigated as expected to occur at different depths on the beams' paths through the irradiated volume. Acute side effects of these partially widened proton minibeams were examined in an in-vivo mouse ear model to account for the immune system, vasculature, and higher complexity.

Methods

A total of six different minibeam sizes were applied to the ear of Balb/c mice using 20 MeV protons. The average dose of 60 Gy was distributed in 4x4 minibeams with beam sizes of σ = 0.09, 0.2, 0.31, 0.45, 0.56 and 0.9 mm and a beam-to-beam distance of 1.8 mm. Inflammatory reactions, i.e. ear swelling and skin reactions, were observed for 90 days after irradiation.

Results

The results show a strong correlation between the applied beam sizes and the dimension of acute side effects after irradiation. The largest beam sizes resulted in significant inflammatory reactions such as ear swelling, erythema, and desquamation within 3-4 weeks after irradiation. The dimension of acute skin reactions was reduced with decreasing beam sizes until almost no ear swelling or other visible skin reactions to the irradiation could be detected.

Conclusion

The results demonstrate that the tissue-sparing effect of proton minibeams is highest for the smallest beam sizes as occurring in the superficial layers of an irradiated volume. The tissue sparing effect decreases with increasing beam size and is smallest for the largest beam size which is equivalent to a homogeneous dose as desired in the target volume. However, since all minibeams have significantly reduced acute side effects compared to broad beam irradiation, proton minibeam radiotherapy may offer various possibilities for innovative approaches in clinical proton radiotherapy.

List of abbreviations

ANOVA	Analysis of Variance
CNS	Central nervous system
DNA	Deoxyribonucleic Acid
DSBs	Double-Strand Breaks
EORTC	European Organisation for Research and Treatment of Cancer
Gy	Gray
keV	Kilo Electronvolt
kg	Kilogram
kV	Kilo Volt
LET	Linear Energy Transfer
LSD	Least Significant Difference
MeV	Mega Electronvolt
mg	Milligram
mm	Millimetre
MRT	Microbeam Radiation Therapy
MV	Megavolt
µm	Micrometre
pMBRT	Proton Minibeam Radiation Therapy
PTCOG	Particle Therapy Co-Operative Group
RBE	Relative Biological Effectiveness
ROS	Reactive Oxygen Species
RTOG	Radiation Therapy Oncology Group
SEM	Standard Error of the Mean
SLDR	Sublethal Damage Recovery
SNAKE	Superconducting Nanoprobe for Applied Nuclear [Kern-] Physics Experiments
SOBP	Spread-out Bragg Peak
WHO	World Health Organisation

Table of Contents

1. Introduction

1.1 Radiation therapy as clinical treatment

Globally, cancer is the second-leading cause of death (WHO/G. Reboux, 2018). The tumour therapy is mainly based on three pillars of treatment: on the one hand, there is surgery as a local therapy option, secondly, there is systemic therapy with chemotherapy and new biological agents, and thirdly, there is radiation therapy. Irradiation is generally considered a local treatment, but stills allows for the treatment of large fields, for example to control microscopic metastases and possibly affected lymphatic tissue around the actual tumour tissue (Wannenmacher M., Debus J., Wenz F., Bahnsen J., 2013). Due to improved therapy options, more than 50 % of adult cancer patients can be treated curatively (Wannenmacher M., Debus J., Wenz F., Bahnsen J., 2013). Of these successfully treated patients, around 50% receive radiation therapy alone or in combination with other treatment options (Wannenmacher M., Debus J., Wenz F., Bahnsen J., 2013). Moreover, radiation therapy is also often employed in palliative care, for example to relieve pain caused by tumour growth or to stabilise bone metastases (Wannenmacher M., Debus J., Wenz F., Bahnsen J., 2013).

1.1.1 Biological effects of ionizing radiation

In tissue, there is usually a well-balanced equilibrium of cell loss and proliferation. In tumours, however, the corresponding growth control mechanisms are defective, allowing for uncontrolled cell proliferation (Weber KJ., 2013). The most important intended effect of ionizing radiation is hence the permanent inhibition of further cell proliferation, which can be considered as a functional cell death (Weber KJ., 2013). It is important to acknowledge that this refers to the suppression of mitotic activity and not to morphological changes as in definitions of apoptosis and necrosis (Weber KJ., 2013). Correspondingly, in the clinical oncological setting, local tumour control is achieved when all clonogenic tumour stem cells are inactivated (Zips, 2010). Therefore, the majority of cell death following irradiation is a result of mitotic catastrophe – it occurs later in time and is not directly caused by the initial response to damage (Wouters, 2010).

As Deoxyribonucleic acid (DNA) is controlled on several checkpoints during the cell cycle, it is also the key target for radiation-induced cell death; double-strand breaks (DSBs) are

the most critical and complex damage for the respective cell to repair and hence the most significant factor in radiation-induced cell killing (Wouters & Begg, 2010).

1.1.2 Normal tissue side effects

Clinical irradiation usually involves healthy tissue both within the tumour volume and in the entrance and exit channel of the irradiation beams. Moreover, certain safety margins have to be kept around the respective tumour volume to account for microscopic – and thus invisible in conventional imaging – infiltration of tumour cells into the surrounding tissue. Also, the planned target volume in clinical radiotherapy usually includes safety margins to account for patients' movements and positioning alterations. Although modern therapy approaches aim to minimise the dose applied to healthy tissue, it is currently not possible to completely avoid it (Dörr W., 2010). Therefore, the occurrence of adverse effects often limits the amount of radiation which can be deposited in the tumour. Thus, it is extremely important to reduce the dose deposition in healthy tissue as far as possible.

Side effects can be classified into acute and late side effects. Differentiation between the two is mainly made according to their latency, the cut-off time is generally defined as 90 days after irradiation (Dörr W., 2010). However, it is important to mention that late effects cannot only be distinguished from early effects by their latency, but also by the underlying biological mechanisms: Early adverse effects can usually be detected in high turnover tissue – such as skin – where an inflammatory reaction is involved and healing is generally complete (Dörr W., 2010). In contrast, late side effects are commonly seen in flexible tissues with no difference between proliferating and functional cells; they take place both in organ parenchyma and in connective and vascular tissue of all organs (Dörr W., 2010). Late side effects are usually accompanied by a reaction of the immune system and mainly irreversible and progressive (Dörr W., 2010).

In this chapter, the focus will be on the acute side effects as only those were monitored in the present study.

According to Dörr, several phases of acute tissue reaction to irradiation can be distinguished (the following paragraph refers to: Dörr W., 2010): at first, the function of affected cells change in terms of intercellular communication due to an increase of pro-inflammatory protein expression. However, the underlying mechanisms are still not well

understood. Further changes including the reduction of progenitor cells and further cell loss due to mechanical stress mainly take place in the stem cell population. Cell depletion together with insufficient cell regeneration results in different grades of hypoplasia, i.e. a reduced number of cells, which can cause clinically apparent symptoms. An important factor for this acute reaction to radiation is the turnover time of the specific tissue. Surviving stem cells – either cells from within irradiated tissue or migrating cells from outside – are responsible for the recovery process after radiation. This process requires more time after the application of higher doses as fewer stem cells survive to take part in the recovery (Dörr W., 2010).

Regarding the particular acute side effects apparent in skin, two main components are to be considered: firstly, erythema can be observed due to radiation effects in the respective vessels which result in vasodilatation; secondly, changes in the epidermal structure, e.g. dry and/or moist desquamation as a result of progressive hypoplasia (Dörr W., 2010). As major changes can develop in relatively short periods, small observation intervals are required for in-vivo experiments to ensure adequate assessment of acute side effects (Dörr W., 2010).

Generally, late side effects like fibrosis are considered more important in radiotherapy as they are usually progressive and not reversible (Dörr W., 2013). However, around 95% of all patients undergoing radiotherapy develop a form of so-called radiodermatitis, i.e. an acute side reaction in the skin (Ryan, 2012). Also, it is acute radiation effects that immediately compromise the patients' quality of life during radiation therapy (Dörr W., 2010). Moreover, some acute side effects – for example severe inflammation of the mucosa in the treatment of head and neck tumours – can also be dose-limiting (Dörr W., 2013). It is hence important to reduce acute side effects, especially in the skin, to further improve radiation therapy.

In addition, some authors state the necessity to consider so-called consequential late effects, i.e. effects that are not acute radiation side effects, but late unfavourable effects following acute side effects (Dörr W., 2013; Dörr W. & Hendry, 2001). As the occurrence and severity of acute side effects can serve as predictive criteria for these consequential late effects, the reduction of acute adverse events can result in amelioration of the patients' long-term situation (Dörr W. & Hendry, 2001).

1.2 Protons in Radiotherapy

1.2.1 Physical properties of proton irradiation

Protons were first suggested to be employed in clinical radiotherapy in 1946 (Wilson, 1946) for their specific physical advantages which make them optimal for radiation therapy. Protons are charged particles and slow down with increasing depth (Joiner, 2010). The respective deposited energy increases along the beam path until the so-called Bragg peak which is where the protons stop in an intense burst of ionization (Joiner, 2010). After the Bragg peak, dose deposition decreases rapidly, which renders the protons' dose distribution profile very convenient for clinical radiation therapy (Dörr W. & Joiner, 2010; Pawlicki, Scanderbeg, & Starkschall, 2016) as virtually no dose is applied to tissue behind the respective target (Dörr W. & Joiner, 2010). For clinical irradiation, the respective energy of the proton is chosen accordingly to the required depth for the Bragg peak to be in the target volume (Schulz-Ertner & Debus, 2013). Covering the entire tumour requires the production of a so-called spread-out Bragg peak (SOBP) by combining proton beams of different energies (Pawlicki et al., 2016). This results in an increased dose in the tissue in front of the target volume. However, the deposited dose in front of the target volume is still far less than in conventional radiotherapy (Joiner, 2010). Thus, the therapeutic window – defined by the ratio of tumour dose to tissue dose – is increased for radiation therapy with protons when compared to conventional radiation therapy with photons (Joiner, 2010). Figure 1 depicts the depth-dose profile of an X-ray beam in comparison with a single proton beam and visualises the creation of the SOBP in the target region.

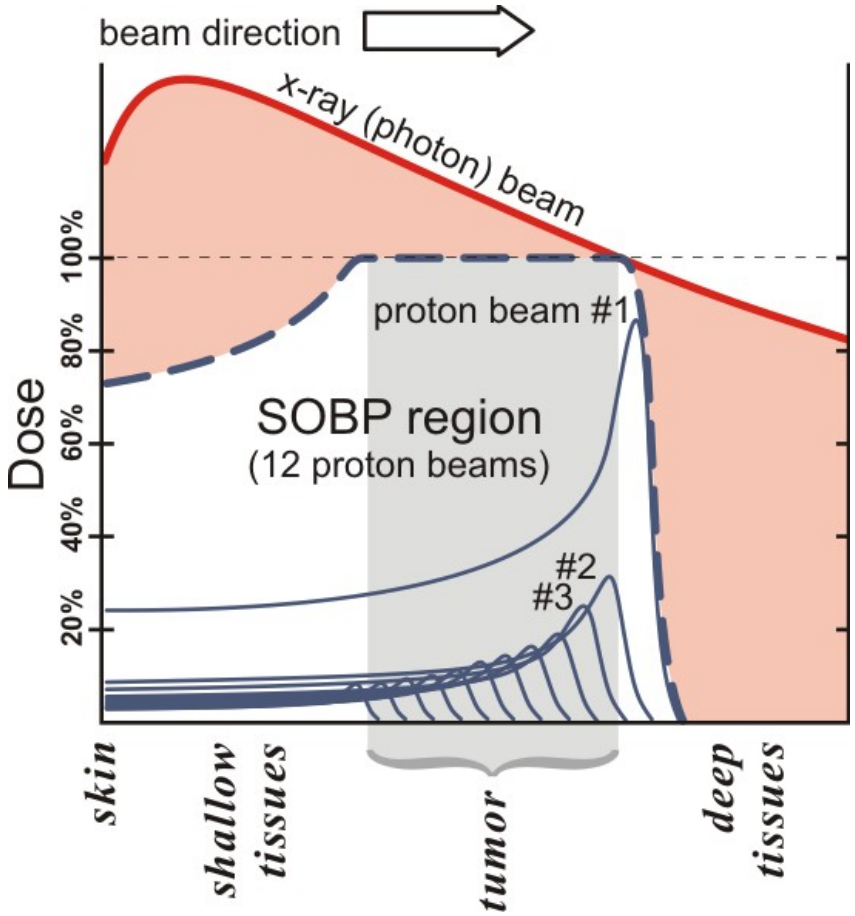

Figure 1: Comparison of dose profiles for proton vs. x-ray radiotherapy. From (MarkFilipak, 2012)

In the concept of spatially fractionated radiation therapy, the small proton beams widen up on their way toward the target volume far more than photons, allowing for virtually homogenous irradiation of a target in a certain depth (Pawlicki et al., 2016; Schulz-Ertner & Debus, 2013).

1.2.2 Biological effects of proton irradiation

To determine the biological effects of any radiation and compare the biological impact, the concepts of linear energy transfer (LET) and relative biological effectiveness (RBE) are employed. LET is defined as the loss of energy of a charged particle per unit length and usually given in the unit [keV/µm] (Girdhani, Sachs, & Hlatky, 2013; Joiner, 2010):

$$LET = \frac{\delta E}{\delta s} \qquad [keV/\mu m]$$

LET depends on the proton beam's energy (Girdhani et al., 2013) and is considered low-LET when the LET is less than 10 keV/µm. Clinically relevant protons are low-LET radiation

for most of their path until the very end of their range (Girdhani et al., 2013), where LET increases drastically up to around 90 keV/µm (Raju, 1995).

RBE is defined as the dose of reference radiation needed to cause a certain biological or clinical effect divided by the dose of the test radiation (in our case protons) required to cause the same effect (Girdhani et al., 2013; Joiner, 2010):

$$RBE = \frac{dose\ of\ reference\ radiation}{dose\ of\ test\ radiation}$$

Generally, either 250 kV X-rays or Co60-γ-rays – which are both low-LET radiation – are used for reference radiation (Joiner, 2010). RBE values are calculated mostly by examining clonogenic survival after irradiation (Girdhani et al., 2013). As clinically used protons show similar effects to photons regarding colony-forming assays, the RBE of clinically used protons is similar to that of photons (Girdhani et al., 2013; Joiner, 2010, p. 77; Weber KJ., 2013). Therefore, the RBE factor of 1.1 has been adopted clinically throughout the spread-out Bragg peak (Paganetti et al., 2002).

However, the uniform RBE value of 1.1 has been in dispute in the last years. Several studies indicate that clonogenic survival does not seem to be the only important factor in the determination of biological effects of particle irradiation; it is important to consider other mechanisms such as via cell-cell interactions and generation of paracrine signals (Girdhani et al., 2013). As explained in chapter 1.1.1, DNA is the key target for ionizing radiation. Proton irradiation has been shown to induce more DNA DSB and so-called clustered lesions – i.e. damage sites that are in close proximity to another, which results in more complex damage patterns – than for example gamma rays or high-energy X-rays (Calugaru et al., 2011; Finnberg, Wambi, Ware, Kennedy, & El-Deiry, 2008; Gerelchuluun et al., 2011). Another report indicates modulation on an epigenetic level in terms of different DNA methylation profiles after exposure to proton irradiation compared to other radiations (Goetz, Morgan, & Baulch, 2011).

It has been shown that proton irradiation can induce more severe damage in tissue than gamma radiation (Green et al., 2001). On a molecular level, several studies demonstrated a faster increase of production of reactive oxygen species (ROS) after irradiation with protons than with photons (Baluchamy et al., 2012; Chang, Zhang, Vassiliev, Gillin, & Mohan, 2010; Giedzinski, Rola, Fike, & Limoli, 2005). The hereby increased oxidative stress

resulted in enhanced apoptotic activity and inhibition of cell proliferation (Baluchamy et al., 2010; Baluchamy et al., 2012; Chang et al., 2010). Thus, several authors suggested different cellular pathways to be activated after proton and photon irradiation, respectively, to account for the different apoptotic or survival reactions (Girdhani et al., 2013; Narang et al., 2009). After proton irradiation, suppression of both angiogenetic signals and inflammatory factors have been demonstrated (Finnberg et al., 2008; Girdhani et al., 2013; Girdhani, Lamont, Hahnfeldt, Abdollahi, & Hlatky, 2012). Also, inhibition of migratory and invasive cell activity was shown (Girdhani et al., 2012; Ogata et al., 2005), although the exact process is not yet fully understood (Girdhani et al., 2013). Nevertheless, especially the impact of proton irradiation on migration and invasion of cells and angiogenesis render proton radiation an interesting approach in radiotherapy and oncology as they could influence tumour growth, recurrence and metastasis even further.

1.2.3 Use in clinical radiotherapy

The advantages of the use of protons in radiation therapy are mainly the physical properties: the increased dose deposition at the end of range of the particle allows for a relatively low dose deposition in the normal tissue between the surface and target volume and the exact calculation of the maximum of energy deposition to the actual tumour (Dörr W. & Joiner, 2010).

Current indications of clinical radiotherapy with protons include paediatric tumours due to the expected reduction of adverse side effects and secondary malignancies in the young patients in spite of the lack of clinical Phase-III trials (Schulz-Ertner & Debus, 2013). However, recent reviews did indicate a certain benefit of proton radiation therapy compared to conventional photon radiation in paediatric tumours of the central nervous system (CNS) (Armoogum & Thorp, 2015; Huynh et al., 2019).

Other indications in adult patients are chondromas/chondrosarcomas and ocular tumours such as choroid melanomas (Schulz-Ertner & Debus, 2013). Also, there may be an advantage in very radioresistant tumours (Schulz-Ertner & Debus, 2013).

Today, clinical radiotherapy with protons is available in about 80 centres worldwide (Particle Therapy Co-Operative Group [PTCOG], 2019). In 2018, over 180000 patients have been treated with protons worldwide (PTCOG, 2019).

Protons are applied either actively via so-called spot scanning or pencil beams or passively using range modulators and collimators (Schulz-Ertner & Debus, 2013). They can be produced either in a cyclotron resulting in a steady, monoenergetic beam or in a synchrotron, where so-called spills of protons are produced for spot scanning (Pawlicki et al., 2016; Schulz-Ertner & Debus, 2013). Range modulation is possible either through varying the energy before the protons leave the accelerator (in the case of the synchrotron) or afterwards via a range modulation wheel with varying thickness (in the case of the cyclotron) and the beam can be magnetically steered (Pawlicki et al., 2016) . The clinically used energy range is between 70 and 250 MeV which allows for a range of about 30 cm in tissue (Pawlicki et al., 2016).

There are several uncertainties to be considered in radiation therapy with protons, especially due to tissue heterogeneities in the human body and anatomic variations (both intrafractionally because of respiration and circulation and interfractionally because of changes in the patient's position) (Pawlicki et al., 2016). Also, the RBE changes along the beam path depending on several factors, resulting in the deposition of low-LET particles with higher energy in the proximal beam path and high-LET particles with lower energy in the more distal parts (Pawlicki et al., 2016). Hence, the RBE varies throughout the spread-out Bragg peak (Pawlicki et al., 2016).

1.3 Spatial fractionation: Mini- and Microbeam radiation therapy in research

Spatial fractionation means the spatial segmentation of the prescribed dose within one fraction. It has been proposed for use in radiation therapy as early as 1909 to allow for the application of higher doses thanks to reduced side effects (Köhler, 1909). More recently, the concept of spatial fractionation has been investigated regarding both X-rays and charged particles. The sparing effects of spatial fractionation are commonly expected to be attributed to the dose-volume effect – i.e., the smaller the irradiated field size, the larger the tolerance of the normal tissue (Peucelle et al., 2015; Withers, Taylor, & Maciejewski, 1988) – and additional bystander effects (Dilmanian F.A. et al., 2007).

The so-called Microbeam Radiation Therapy (MRT) was first introduced at the Brookhaven National Laboratory in New York, NY, USA (Serduc et al., 2008) and further investigated and developed at the European Synchrotron Radiation Facility in Grenoble, France (Bräuer-Krisch et al., 2003; Bräuer-Krisch et al., 2005; Laissue, Blattmann, Wagner, Grotzer, &

Slatkin, 2007). MRT uses arrays with several highly energetic photon beams with distances of 50-400 µm. The beam pattern is kept throughout the target volume as there is almost no lateral scattering of the photon beams; i.e. dose deposition is not homogenous in the target volume as in conventional radiation therapy. Nonetheless, it was possible to achieve a certain tumour control after irradiation of the brains of 9L gliosarcoma bearing rats (Dilmanian F.A., 2002). To obtain a homogenous dose within the target, the interlacing of several beam arrays from different directions has been proposed (Serduc et al., 2010). As ions – especially heavy ions – show a favourable dose distribution profile compared to photons due to the formation of a Bragg peak and distal dose fall-off, the same principle of microbeam irradiation has been proposed employing carbon ions (Dilmanian F.A. et al., 2012).

The other main fundamental concept introduced in the last years is the so-called Proton Minibeam Radiation Therapy (pMBRT) using slightly larger proton beams with distances of a few millimetres (Prezado Y. & Fois, 2013; Zlobinskaya et al., 2013). Due to multiple Coulomb scattering and hence gradual broadening of the proton minibeams with increasing track length (as explained above), a homogenous dose is applied to the target volume if the beams' variables are chosen accordingly. The Proton Minibeam Radiation Therapy approach has been shown to spare normal tissue around the respective target volume in in-vivo models (Girst et al., 2016; Prezado Y. et al., 2017). Its physical feasibility in existing proton therapy centres has been proven in several studies (Dilmanian F.A., Eley, & Krishnan, 2015; Peucelle et al., 2015).

1.4 Purpose of the investigation

In this study, the effect of partially widened proton minibeams was investigated. The corresponding minibeam sizes were chosen as expected to occur at different depths on their way through the irradiated volume. In figure 2, the different levels of proton minibeams are exemplified through the green circles – note that these are not positioned true to scale (figure modified from (Meyer et al., 2019)). Hereby, the tissue-sparing effect of pMBRT that has been observed in previous studies was to be further analysed. An in-vivo tumour-free mouse ear model was chosen to account for the immune system, vasculature, and higher complexity in living tissues. After irradiation with proton minibeams of several sizes, the acute side effects were observed and quantified in the irradiated murine ears.

Most of the results and ideas presented in this doctoral thesis have already been published in (Sammer et al., 2019). This results in similarity of the used expressions, which is sometimes inevitable.

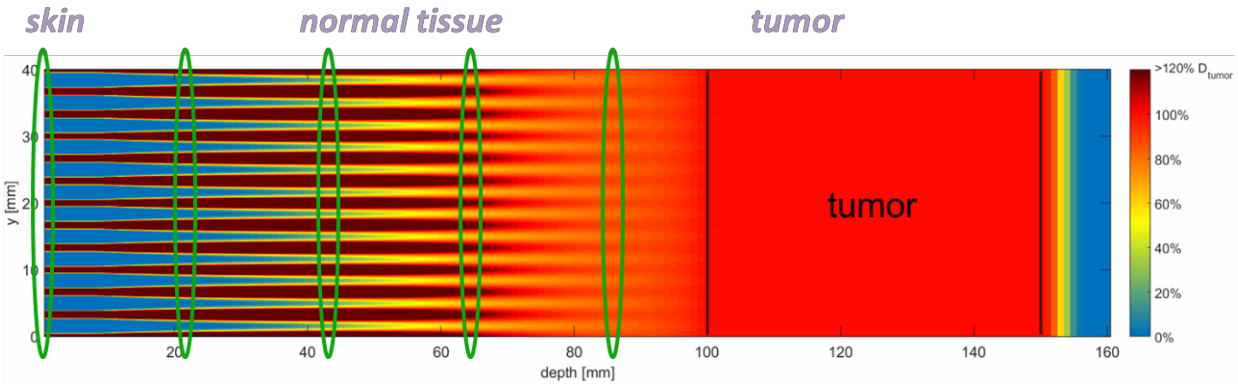

Figure 2: Schematic outline of the levels of proton minibeams investigated in this study. Figure modified from (Meyer et al., 2019).

2. Material and Methods

2.1 Animal model and ethics statement

Female BALB/C mice (Charles River Laboratories, Sulzfeld, Germany) at the age of 6 to 8 weeks were used as tumour-free animal model. These were chosen because of their relatively large and thin ears with an average thickness of about 220 µm, allowing for both good observation of changes to the ear morphology and exact calculation of dose deposition.

From the 14th of January 2015, the 58 mice were housed in 12 standard cages with five mice per cage. The mice were transferred to new cages with new litter once a week and their well-being was controlled every day. Also, food and water supplies were checked and restored daily. For each cage, the mice's tails were marked with one to five lines in four colours to distinguish them.

The District Government of Upper Bavaria approved of all animal experiments, which were performed in accordance with the animal welfare and ethical guidelines of our institutions (ROB Az. 55.2.1.54-2532-144-13).

2.2 Irradiation at SNAKE (Superconducting nanoprobe for applied nuclear physics experiments)

The mice were divided up into six beam size groups (with Gaussian-shaped beam size σ = 0.09, 0.2, 0.31, 0.45, 0.56 and 0.9 mm) and one control group (= sham group). Two mice served as reserve after scheduled irradiation could not be ensured in two cases (mouse no. 4 and no. 19).

Irradiation took place at the Munich ion microprobe SNAKE of the 14 MV Munich tandem accelerator which has been specially adapted to suit biological experiments with animals and has been used in previous studies by our group (Girst et al., 2015; Girst et al., 2016; Greubel et al., 2008; Greubel et al., 2011; Hauptner et al., 2004; Zlobinskaya et al., 2013). Similar to previous studies, a 200 µm aluminium layer on the exit nozzle of the microprobe was used to create the respective beam sizes through the scattering of the microbeam.

During the preparation of irradiation, each mouse was anaesthetized injecting Medetomidine (0.50 mg/kg) + Midazolam (5.0 mg/kg) + Fentanyl (0.05 mg/kg) intraperitoneally before being placed in a specially designed prewarmed aluminium container to allow for irradiation of the right ear and shield the body from radiation. The right ear was secured into a frame by adhesive tape to ensure the target area to lie flat and be aimed at easily. Radiochromic EBT3 films (GafChromicTM, Ashland, US) were then attached on one side of the ear. The eyes were covered with Bepanthen Eye and Nose ointment to prevent them from dehydrating. Each mouse was then carried to the hall containing the scanning microprobe and put in front of the beam with the radiochromic film facing away from the beam.

It was then irradiated with 20 MeV protons according to the previously assigned beam size group (see table 1 for respective beam size groups).

Beam size	Sham	0.09 mm	0.2 mm	0.31 mm	0.45 mm	0.56 mm	0.9 mm	Drop out	Total
Mouse Nos.	7, 14, 21, 28, 38, 42, 47, 49	1, 8, 15, 22, 29, 35, 43, 50	2, 9, 16, 23, 30, 36, 45, 51	3, 10, 17, 24, 31, 37, 44, 52	11, 18, 25, 32, 39, 46, 53, 57	5, 12, 26, 33, 40, 54, 56, 58	6, 13, 20, 27, 34, 41, 48, 55	4, 19	n = 58

Table 1: Distribution of mice to the various beam size groups.

The minibeam pattern comprised 4x4 beams with a centre-to-centre distance of 1.8 mm on a total irradiation field of around 7.2x7.2 mm (as in the previous study by our group, cf. (Girst et al., 2016)). Every single beam consisted of ~4.58 x 10^8 protons, resulting in a mean total dose of 60 Gy applied to the irradiation field. The LET of the applied 20 MeV protons with a range of ~4.6 mm is around 2.7 keV/µm in the irradiated ears. After passing through the ear, the protons were counted by a scintillator-photomultiplier detector. High particle count rates (in the MHz range) were required due to the maximum irradiation time of around 30 min (determined by a maximum time for anaesthesia of around 45 min). Correction of the resulting dead times of detector and detection electronics was performed through radiochromic films for exact dosimetry. These can also serve for visualization of the respective beam patterns (see figure 3 for photographs of radiochromic films; the photographs were taken immediately after irradiation). Mice belonging to the control group were not irradiated, but only anaesthetized and set into the container to imitate the other mice's treatment.

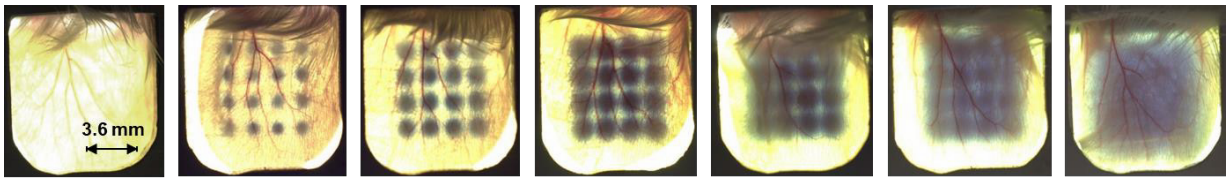

Figure 3: Photographs of radiochromic films showing the different beam application modes (cf. (Sammer et al., 2019)).

After the irradiation, Atipamezole (2.5 mg/kg) + Flumazenil (0.5 mg/kg) + Naloxone (1.2 mg/kg)) were injected subcutaneously to each mouse to recover from anaesthesia. Afterwards, mice were placed back into their previous cage. After recovery, the mice were transported back to a quarantine area at the Klinikum rechts der Isar.

2.3 Observation of acute inflammatory response over 90 days after irradiation

The acute inflammatory response was monitored over 90 days after the irradiation (time after irradiation is the average of days after irradiation for the respective beam size groups – hence Day 0, 4, 9, 12, 15, 17, 19, 21, 22, 23, 24, 25, 26, 27, 28, 29, 30, 31, 33, 35, 37, 39, 43, 47, 54, 59, 68, 75, 82, 88). At each day of measurement, each ear was sized in thickness three times to reduce measuring errors. The measurement was taken by using a specially adapted electronic external measuring gauge (C1X079, Kroplin GmbH, Schluchtern, Germany) with measuring contacts of 6mm diameter (see figure 4).

Figure 4: Measuring gauge used for measurements of ear thickness.

Severity of erythema (Score A) and dimension of desquamation both on the inside and on the outside of both ears (Score B) were assessed using a previously defined scale. These data were then transformed into a numeric score (see table 2) which is based on clinically implemented criteria defined by the Radiation Therapy Oncology Group (RTOG), the European Organisation for Research and Treatment of Cancer (EORTC) and the World Health Organisation (WHO) (Cox, Stetz, & Pajak, 1995; Seegenschmiedt, 2013). This score has been used in our laboratory in previous studies (Girst et al., 2016).

Score A	Erythema	Score B	Desquamation
0	none	0	none
0.5	mild erythema	1	dry desquamation
1.5	definite erythema	2	crust formation
3	severe erythema	3	moist desquamation

Table 2: Numeric score of the inflammatory reaction (modified from (Girst et al., 2016)).

Also, the ear morphology and possible hair loss were evaluated. The mice's weight, general condition, and signs of pain were also observed.

The measurements were always taken by two persons and the order in which the cages were evaluated was changed at every day of measurement. The person knowing which cage was currently being observed did not know the mice's respective beam size group to avoid personal bias.

Photographs of selected mice's ears were taken on days 0, 15, 26, 35 and 88 to illustrate the visible inflammation reaction.

The well-being and behaviour of the mice were controlled according to the scoring guidelines of the animal application.

2.4 Statistical analysis

All statistical analyses were conducted with IBM SPSS 25 software and Microsoft Excel of Microsoft Office 365 ProPlus.

Baseline values of the right ear thickness were visualised with box plot graphs. Right ear thickness over the observation period of 90 days was analysed with the one-way analysis of variance ANOVA for repeated measures to verify differences in right ear thickness values between the different beam size groups. LSD (Least significant difference) was used as a Post-hoc test to account for multiple testing for comparison of the different groups. The difference of averaged values for each beam size group to the baseline values was calculated at each time point to correct for possible discrepancies in baseline values between the beam size groups and thus to allow for more precise evaluation. The values for change in thickness obtained were then again analysed with the ANOVA for repeated measures and LSD as a Post-hoc test.

Pearson's correlation coefficient was calculated for investigation of the association between maximum ear thickness and beam size group and the association of relative maximum increase in ear thickness and beam size group, respectively. For comparison of thickness values at the end of the observation period, a mean value of the last five measurements (e.g. day 88, 82, 75, 68, 59) was calculated for each mouse and then compared by beam size group using the one-way ANOVA with Greenhouse-Geisser correction and LSD test. Also, a mean value of change in ear thickness per beam size group was calculated over the last five measurements and associated with the beam size group by calculation of Pearson's correlation coefficient.

Erythema and desquamation were combined into a total score by adding up the erythema value and the respective maximum desquamation score value. These were then analysed with one-way ANOVA for repeated measures and LSD as explained above. As the baseline inflammation score of 0.0 was obtained for all beam size groups, no further calculations were necessary to correct for differences in baseline values. The association between maximum score and beam size group was investigated by calculation of Pearson's correlation coefficient.

3. Results

3.1 Ear Thickness

3.1.1 Left Ear Thickness

Left ear thickness was measured at every observation point to serve as an internal control. It did not vary relevantly over the observation period (cf. figure 5). Thus, in the following paragraphs, ear thickness will always refer to the right ears' thickness values.

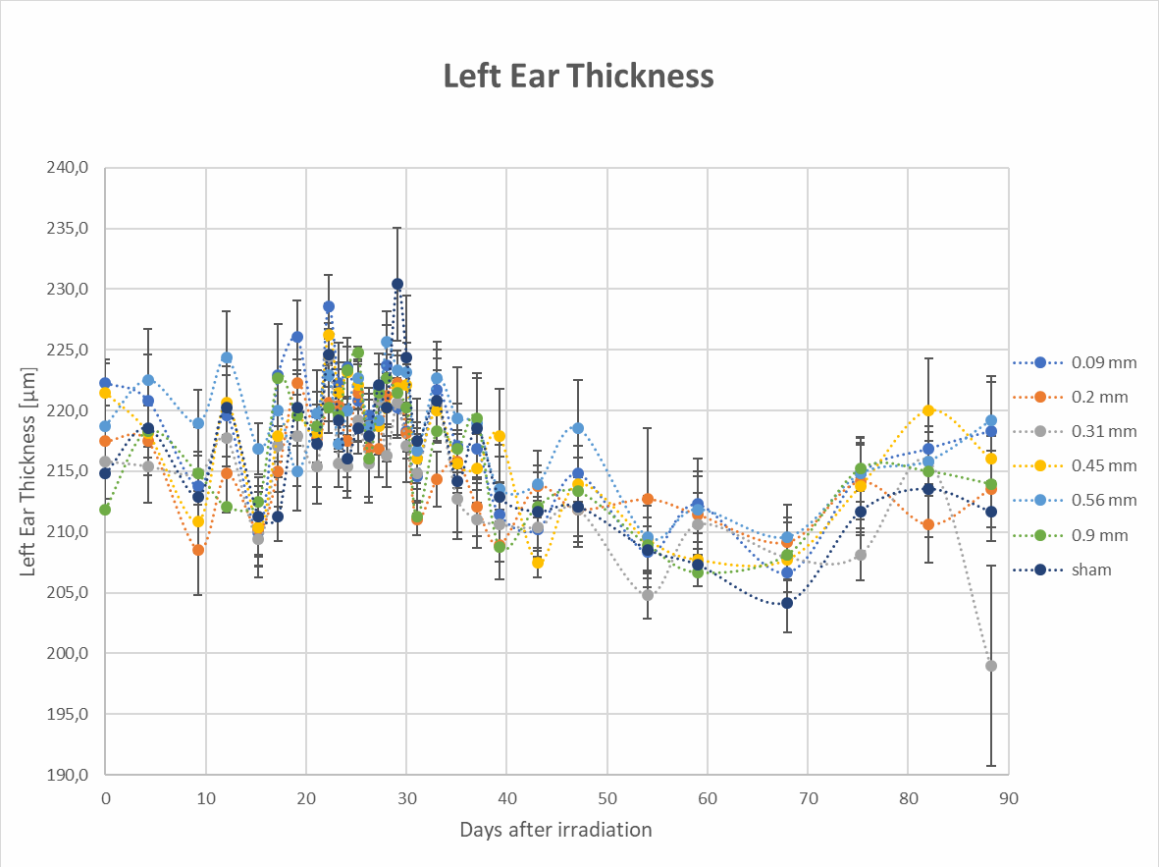

Figure 5: Left Ear Thickness over the 90 days of observation. Error bars represent Standard Error of the Mean (SEM).

3.1.1 Right Ear Thickness

Before irradiation, right ear thickness was about the same for all beam size groups with a mean over all groups of 219.8 µm +- SEM 1.0 µm (cf. figure 6).

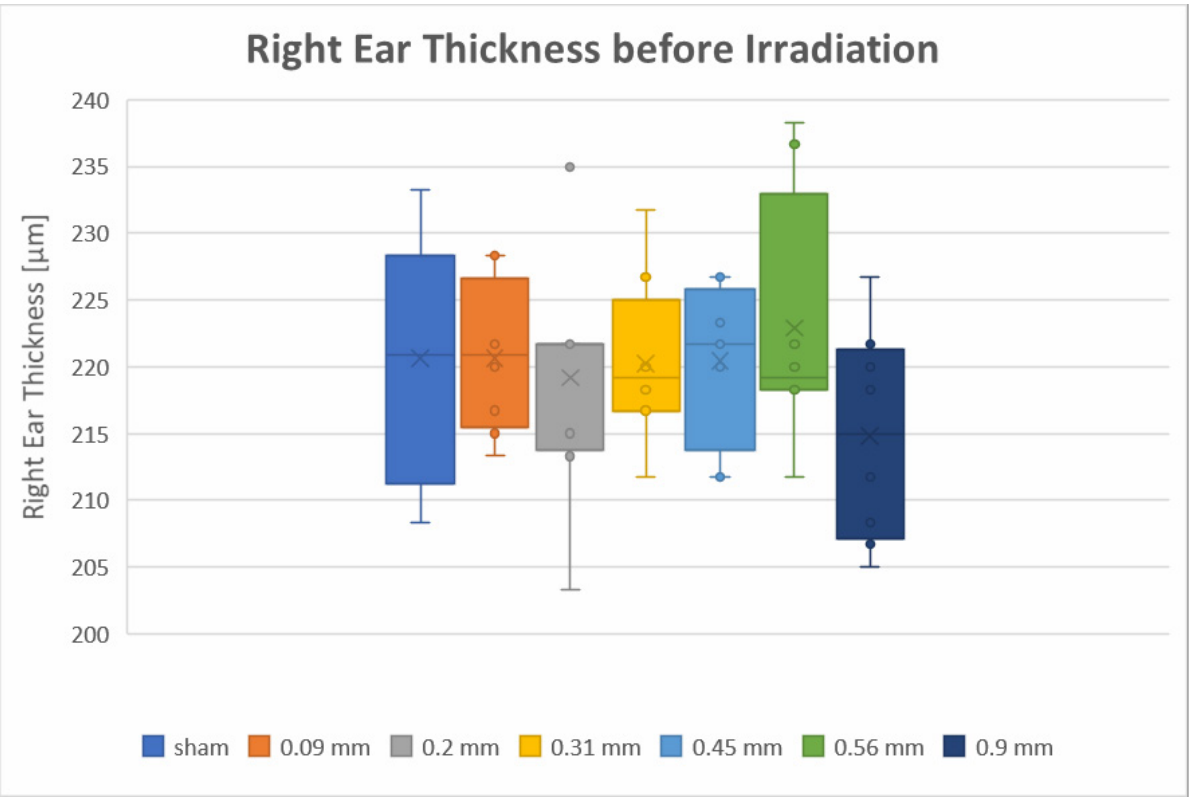

Figure 6: Right ear thickness in the various beam size groups before irradiation. Error bars represent SEM.

No change in ear thickness was seen in the sham irradiated group. Likewise, when compared to the control group, no statistically significant increase in ear thickness could be detected in the group irradiated with the beam size σ = 0.09 mm (p = 0.584). All other beam size groups were found to differ statistically significantly from the control group in both absolute ear thickness values during the observation period (p=0.023 for 0.2 mm, p=0.001 for 0.31 mm, p<0.001 for 0.45, 0.56 and 0.9 mm beam size groups) and change in ear thickness compared to the respective baseline values (p=0.022 for 0.2 mm, p=0.001 for 0.31 mm, p<0.001 for 0.45, 0.56 and 0.9 mm beam size groups; cf. figure 7 and 8). With increasing beam size, the maximum reaction in ear thickness rises, with a maximum of two- to threefold thickness (mean values are 526.7 µm for 0.56 mm vs. 230 µm for sham).

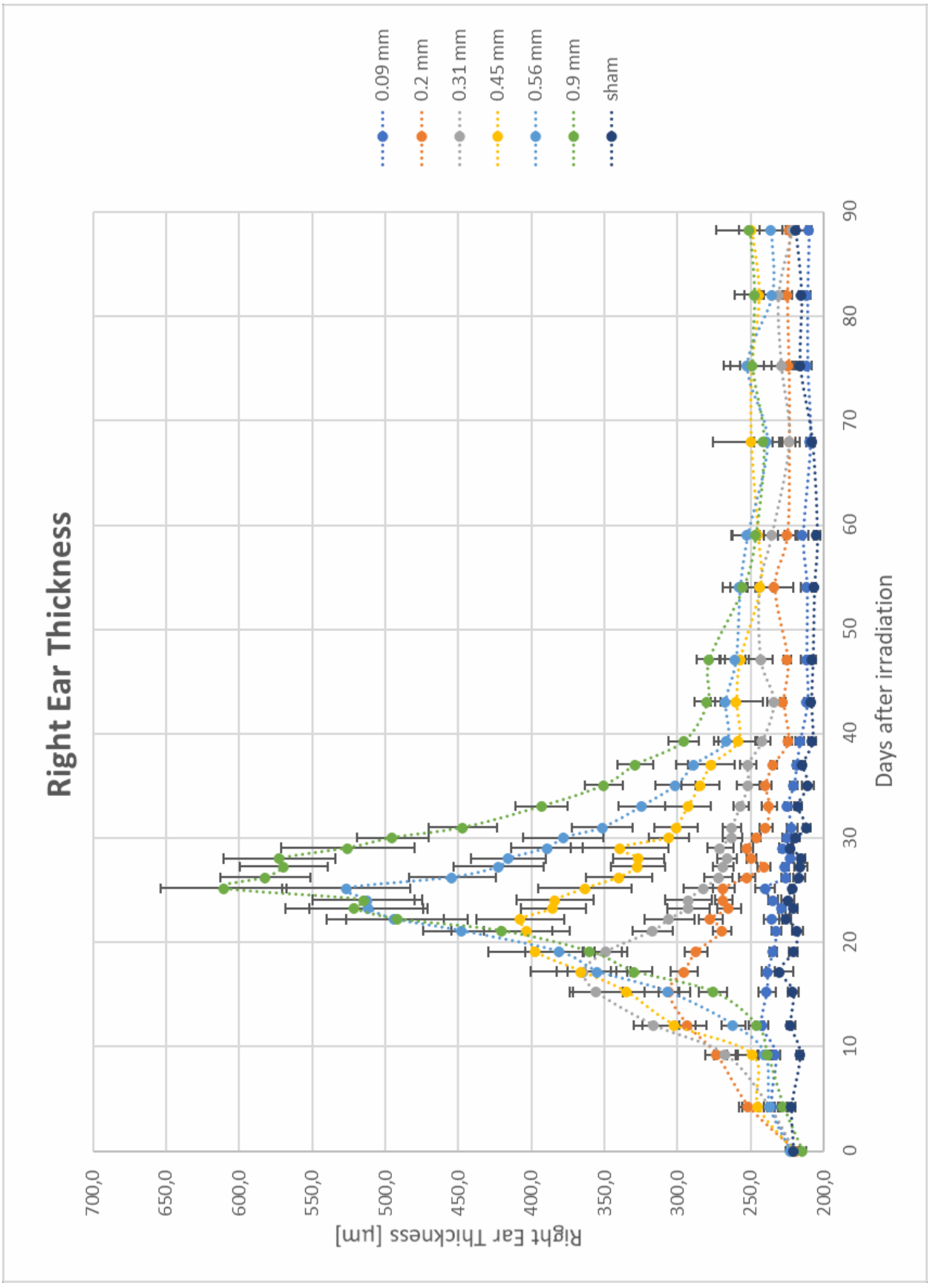

Figure 7: Right ear thickness plotted against days after irradiation. Error bars represent SEM.

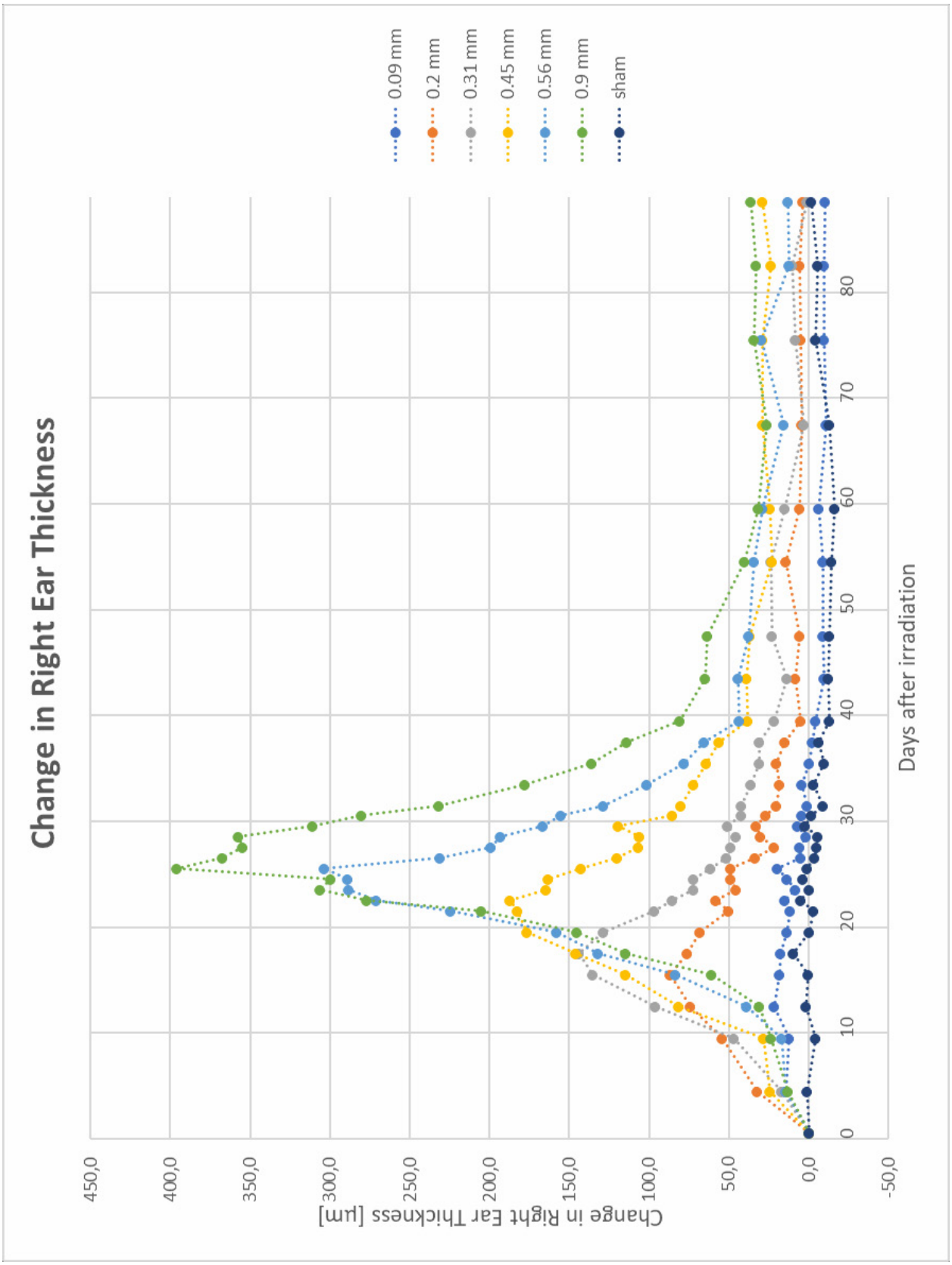

Figure 8: Change in right ear thickness compared to the respective beam size groups' baseline values.

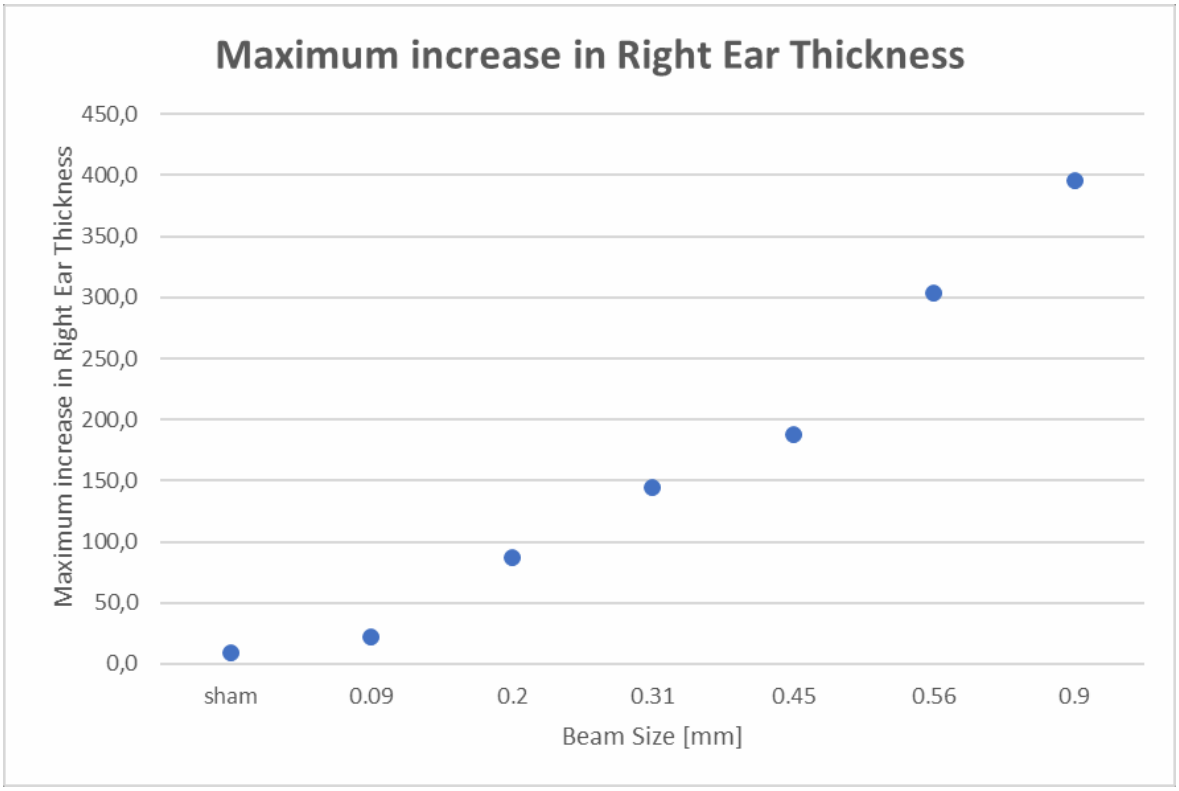

Figure 9: Maximum increase in right ear thickness per beam size group compared to the respective group's baseline values.

Figure 9 visualises the maximum increase in ear thickness per beam size group compared to the respective baseline values. The maximum increase in ear thickness is around +300 µm for the 0.56 mm beam size group (vs. around +10 µm for the sham irradiated group, $p<0.001$ for comparison between the 0.56 mm and sham irradiated group). A strong correlation between applied beam size and maximum increase in ear thickness was shown (Pearson's correlation coefficient 0.986, $p<0.001$). Also, a significant increase in ear thickness was observed in the 0.9 mm beam size group – i.e. corresponding to homogenous irradiation – in comparison with all the minibeam applications ($p=0.026$ for comparison of 0.56 mm and 0.9 mm group). In absolute numbers, the results show a strong correlation between applied beam size and maximum mean ear thickness within each beam size group (Pearson's correlation coefficient 0.984, $p<0.01$, see figure 10).

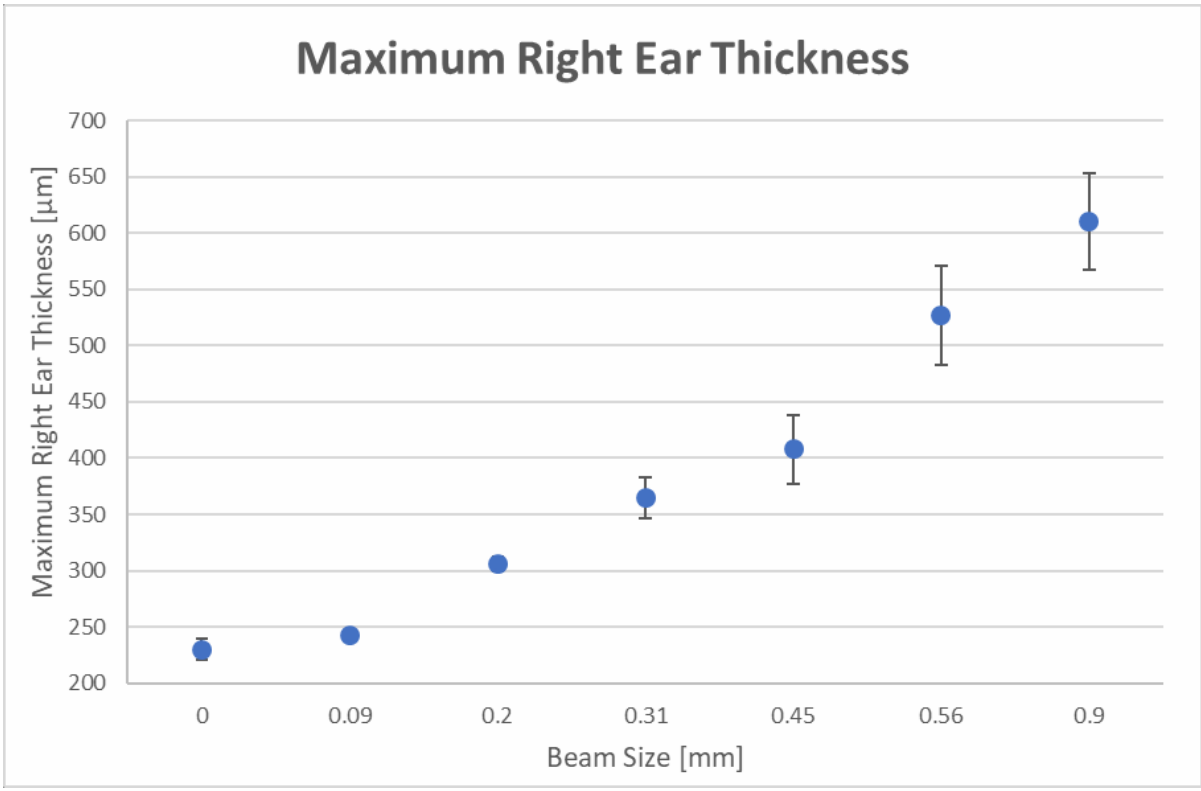

Figure 10: Maximum right ear thickness plotted against beam size. Error bars represent SEM.

The maximum reaction also shifts toward later time points with increasing beam size. While the ear thickness reaches a maximum after approximately 15 days in the 0.09 mm beam size group, the reaction hits the peak later around day 25 in the 0.9 mm beam size group.

After the peak, the ear thickness decreases and reaches control values approximately at day 55 for the sham group and the smaller beam size groups up to the 0.31 mm group. However, detumescence takes longer for larger beam sizes than for smaller beam sizes. Moreover, recovery is not completed for the bigger beam size groups at the end of the observation period: whereas thickness values fully decrease back to the baseline values for the smaller beam size groups, they level off at 247.4 µm +- 1.2 µm SEM (difference to initial value +27 µm) for σ = 0.45 mm, at 243.0 µm +- 3.9 µm SEM (difference to initial value +20.1 µm) for σ = 0.56 mm and at 247.0 µm +- 1.7 µm SEM (difference to initial value +32.2 µm) for σ = 0.9 mm (ear thickness values are averaged values of the last five measure points). Figure 11 visualises absolute ear thickness values for the end of the observation period.

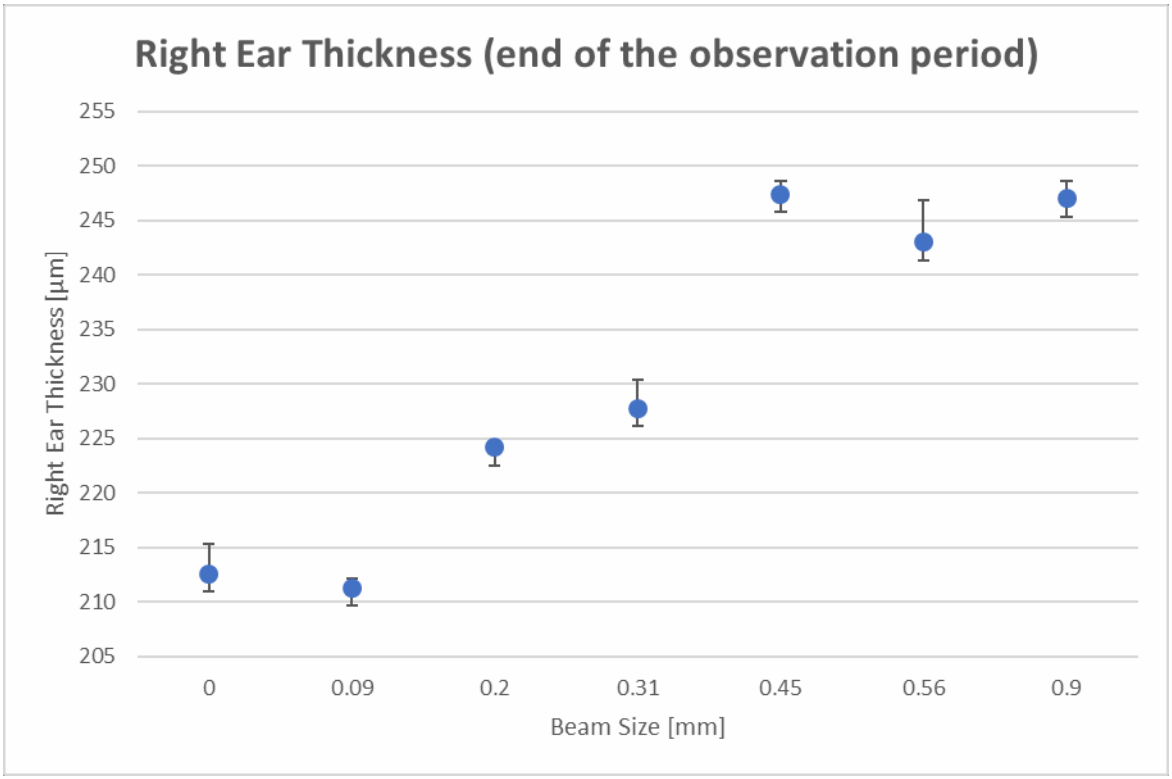

Figure 11: Right ear thickness at the end of the observation period plotted against beam size. Error bars represent SEM.

Averaged absolute values at the end of the 90 days' observation period are significantly higher for the 0.45 mm (mean difference to the sham group = +34.8, p=0.01), the 0.56 mm (mean difference to the sham group = +30.4 µm, p=0.024) and the 0.9 mm beam size group (mean difference to the sham group = +34.4 µm, p=0.011) compared to the sham irradiated control group (cf. figure 11).

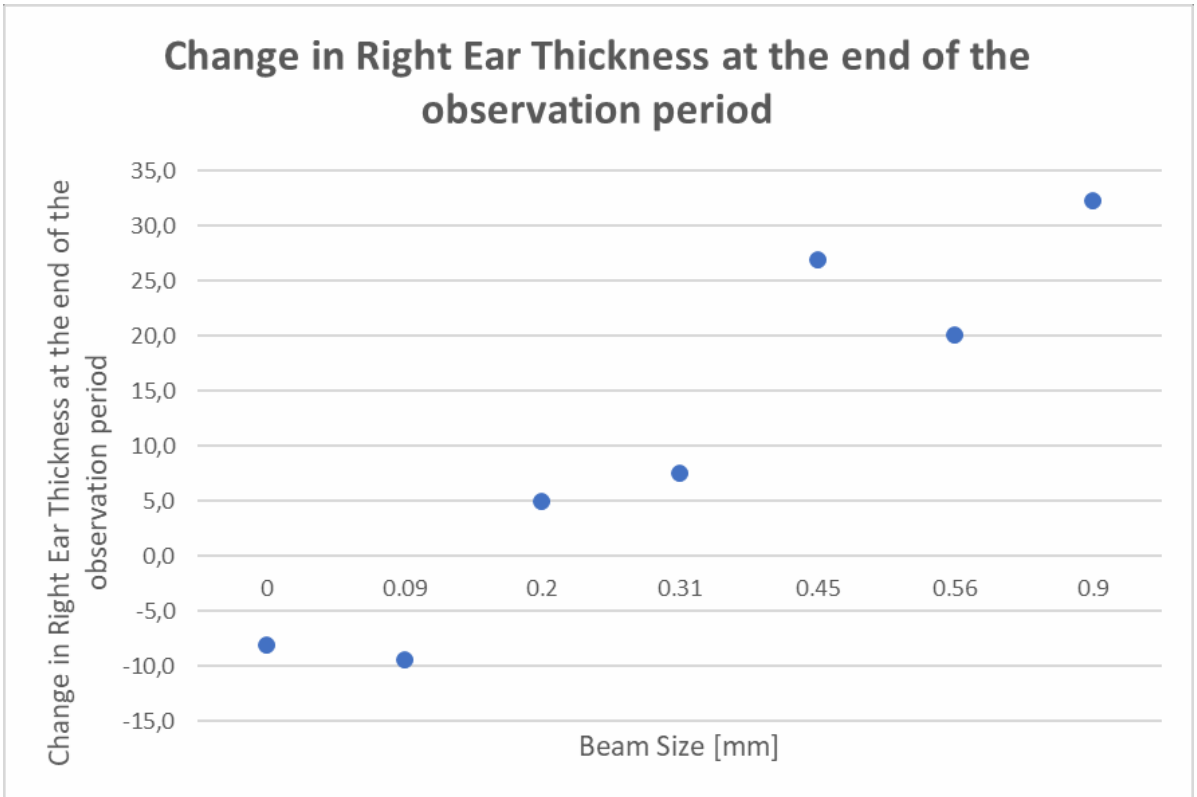

Figure 12: Change in right ear thickness at the end of the observation period per beam size group in relation to the respective group's baseline values.

Figure 12 visualises the different beam size groups' relative values at the end of the observation period (compared to the respective baseline values). The results show a strong correlation between applied beam size and change in ear thickness per beam group in relation to the respective baseline values with a Pearson's correlation coefficient of 0.930 (p=0.002). For the sham irradiated and the 0.09 mm group, negative values – i.e., decrease in ear thickness – were obtained at the end of the observation period. For the 0.2 and 0.31 mm group, ear thickness increased only minimally compared to their baseline values (approx. +5 µm for the 0.2 mm beam size group and +8 µm for the 0.31 mm beam size group). For the bigger beam size groups, ear thickness increased more prominently with approx. +27 µm for the 0.45 mm group (p=0.016 compared to sham irradiated group), approx. +20 µm for the 0.56 mm group (p=0.052 compared to sham irradiated group) and approx. +32 µm for the 0.9 mm group (p=0.006 compared to sham irradiated group).

3.2 Right Ear Inflammation score

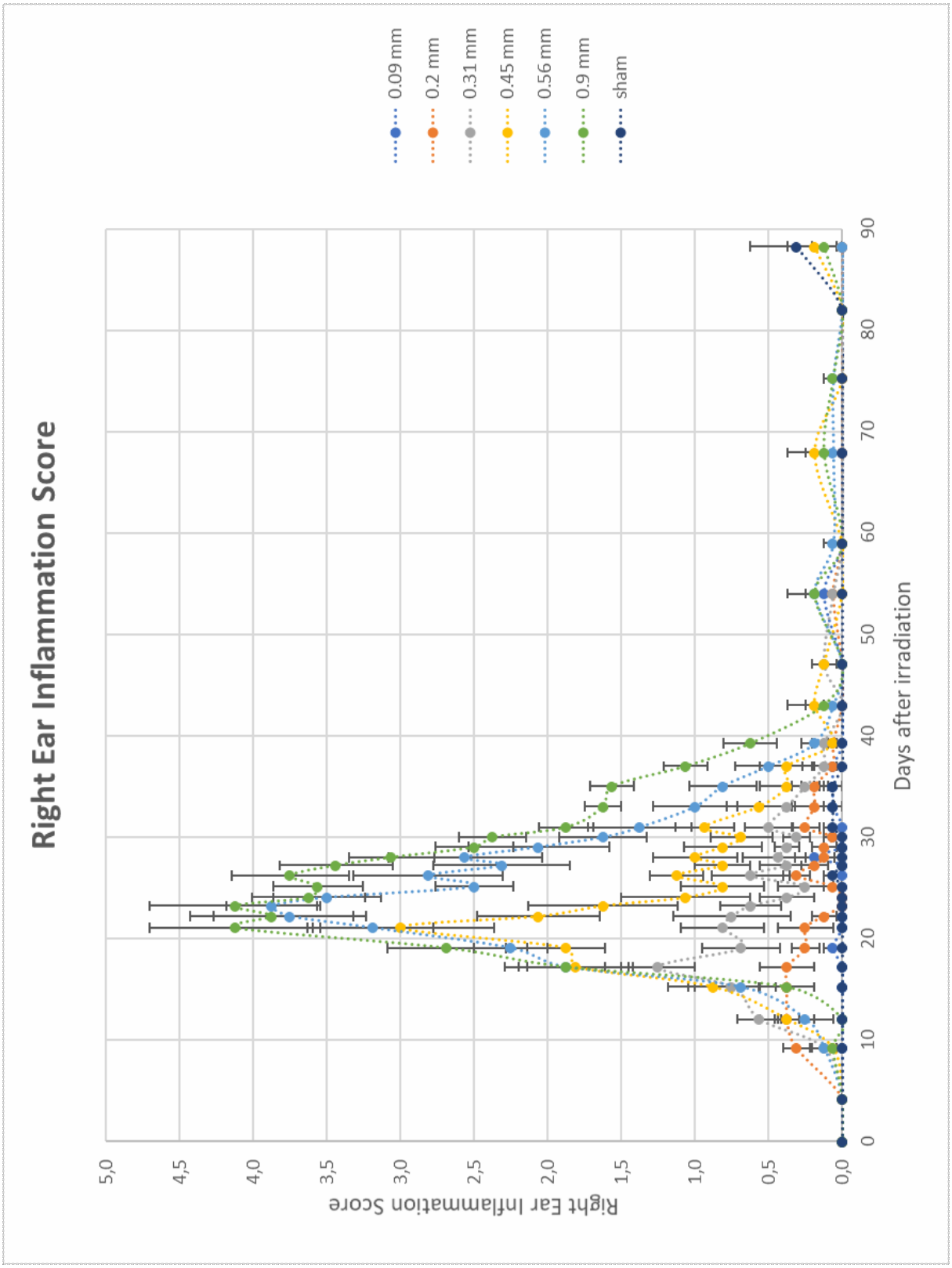

Figure 13: Right ear inflammation score plotted against days after irradiation. Error bars represent SEM.

Figure 13 visualises the overall trend of inflammation score per beam size group during the observation period. No or only very discreet inflammation reaction in terms of erythema and desquamation could be detected in both the 0.09 mm and the 0.2 mm beam size groups in comparison with the control (=sham) group. Thus, no significantly increased inflammation score was observed. For the larger beam size groups, a significantly increased inflammation score was detected, resulting in a maximum score of around four times the baseline value for the 0.56 mm beam size group compared to the sham group ($p < 0.01$, see figure 14). The results show a strong correlation between applied beam size and maximum inflammation reaction (Pearson's correlation coefficient 0.931, p=0.002).

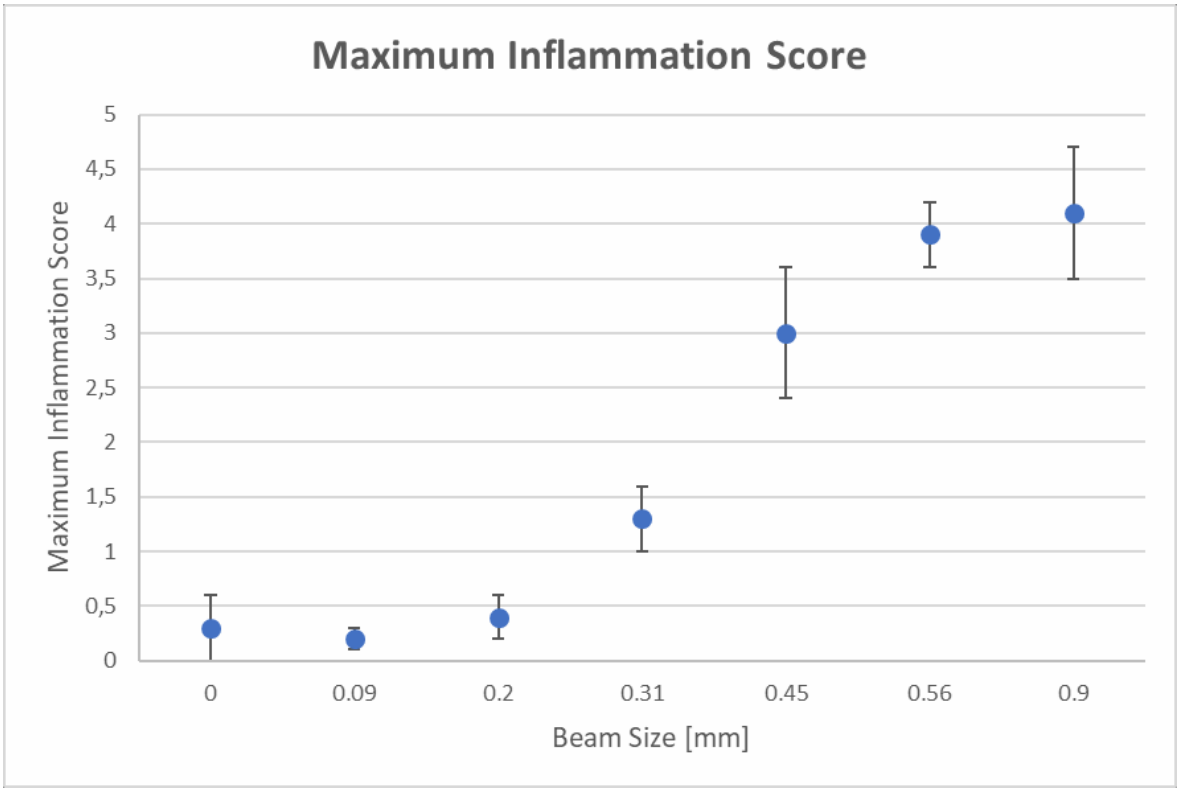

Figure 14: Maximum inflammation score plotted against beam size group. Error bars represent SEM.

When comparing the time points of maximal inflammation reaction, both erythema and desquamation tend to reach their maximum slightly before the maximum ear thickness is obtained. Both erythema and desquamation were completely reversible and were not detected anymore at the end of the observation period.

3.1.1 Right Ear Erythema (Score A)

For the sham and 0.09 mm beam size group, no visible erythema could be detected during the observation period. In the other beam size groups, the onset of erythema started around day 12-15. For the 0.2 mm and 0.31 mm group, means of maximum erythema scores of 0.4 and 0.6 were found on days 12 and 17, respectively, indicating mild erythema as a maximum reaction. In the 0.2 mm group, erythema was declining around day 30 whereas recovery did not start until around day 35 in the 0.31 mm group. For the three largest beam size groups (0.45, 0.56, and 0.9 mm), means of maximum erythema scores between 1.4 and 2.0 were obtained on days 21-24, indicating definite to severe erythema formation. Here, the healing process was not complete until around day 40. Nonetheless, recovery from erythema was complete at the end of the observation period resulting in no visible erythema on day 88 (cf. figure 15).

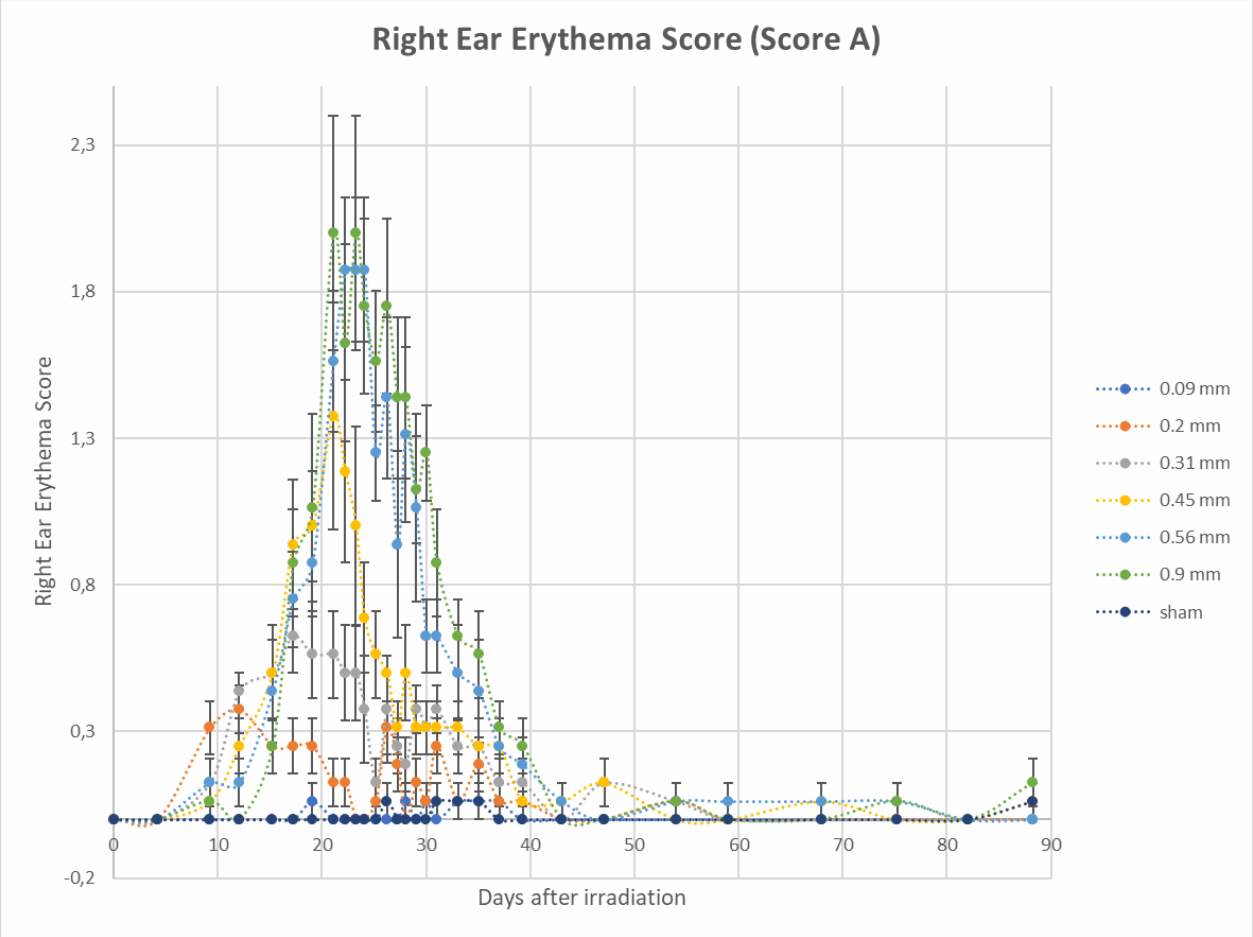

Figure 15: Right ear erythema score plotted against days after irradiation. Error bars represent SEM.

3.2.2 Right Ear Desquamation (Score B)

No desquamation was observed in the sham, 0.9 mm, and 0.2 mm beam size group. For the 0.31 mm beam size group, a maximum desquamation score of 0.6 was obtained on day 17. For the three largest beam size groups (0.45, 0.56 and 0.9 mm), scores from 1.6 to 2.3 were observed on days 21-23, indicating dry desquamation or crust formation (cf. figure 16). In addition, moist desquamation was present in several animals in both the 0.56 mm and the 0.900 µm beam size group around the time points of maximum inflammation reaction as shown in representative photographs of maximum inflammation reaction in figure 17. For these biggest beam size groups, recovery took longer and was complete around day 40. At the end of the observation period, no desquamation could be detected in the irradiated ears (cf. figure 16).

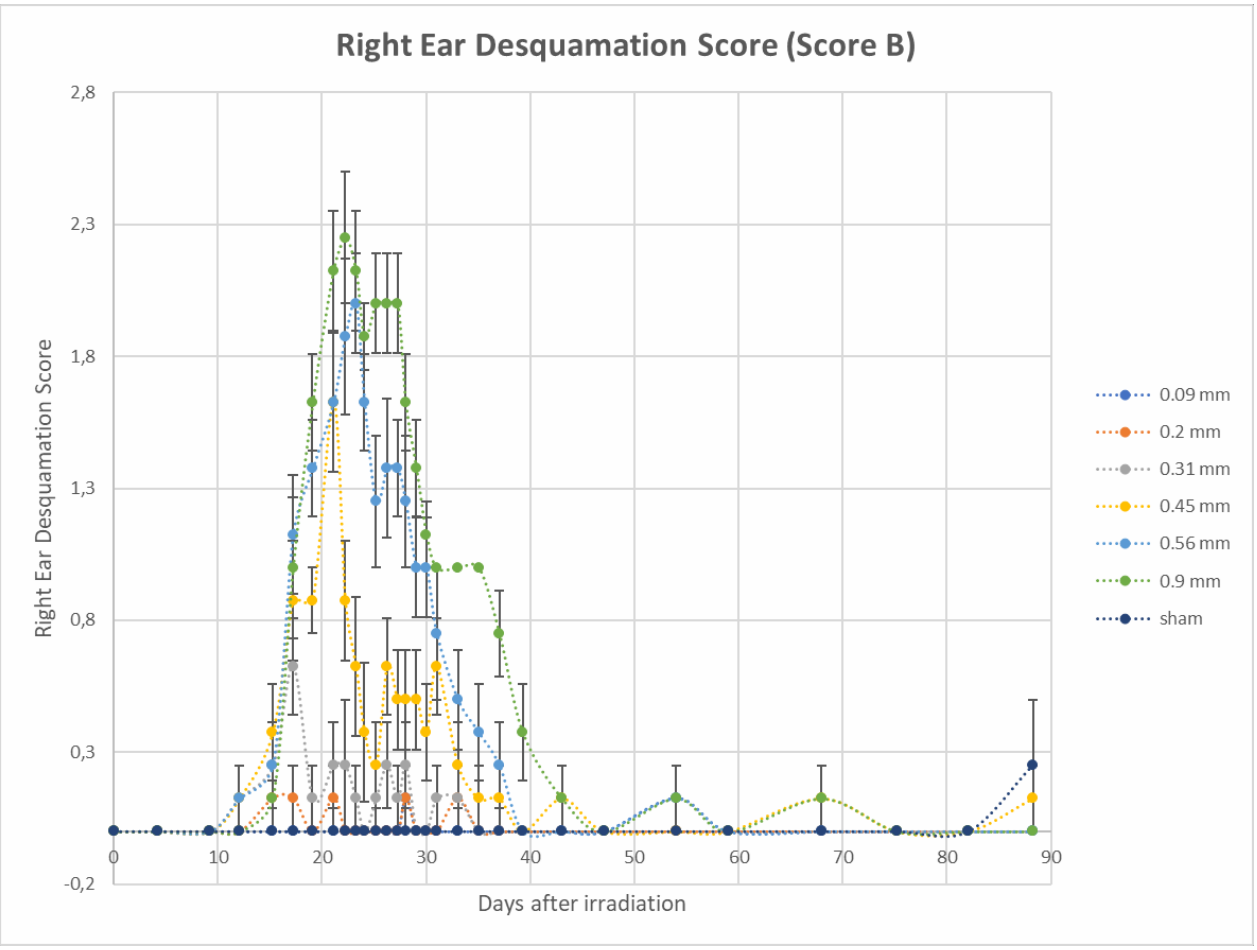

Figure 16: Right ear desquamation score during the observation period of 90 days. Error bars represent SEM.

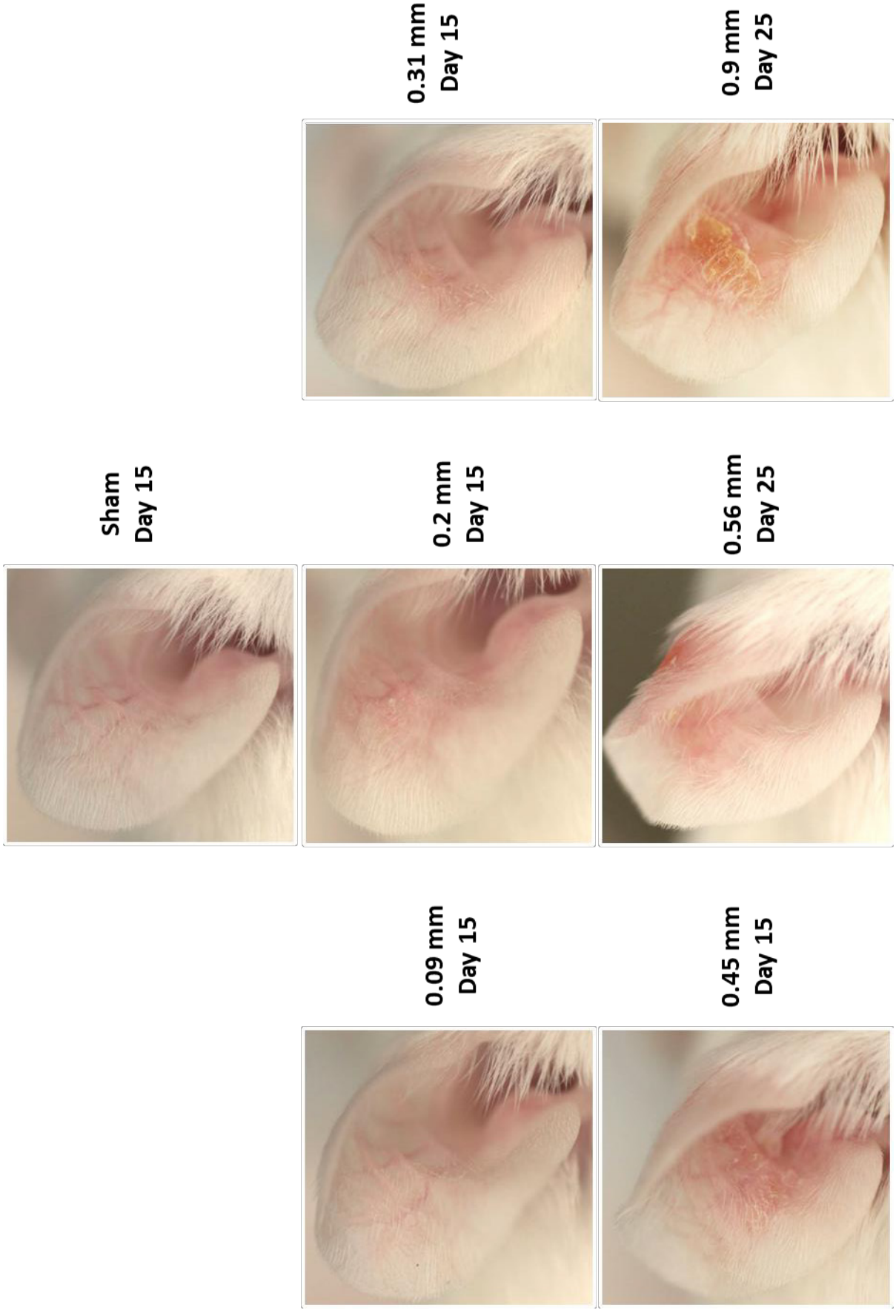

Figure 17: Photographs of the maximum inflammatory skin reaction per beam size group.

3.3 General remarks

No hair loss was detected in any of the mice during the monitoring period. Only four mice showed signs of mild pain about three weeks after irradiation. In three mice, defence reactions were noticed around the days of maximum reaction. A general tendency of all mice to gain weight could be seen during the 90 days of monitoring.

4. Discussion

The present results demonstrate that Proton Minibeam Radiation Therapy (pMBRT) offers the opportunity to spare normal tissue. As described above, the tissue-sparing effects of proton minibeams are higher for smaller beam sizes as they would occur in superficial layers of an irradiated volume. As the beam size increases with depth through the entrance channel, the tissue-sparing effect decreases until an effect similar to that of homogenous irradiation is obtained for the theoretical target volume.

The formation of erythema was seen to begin slightly before desquamation, and both erythema and desquamation reached their maximum values before the maximum ear thickness was obtained. These findings correspond to those made in other studies on the same animal model (Dombrowsky et al., 2019; Girst et al., 2016). Also, the trend of the inflammatory reaction of the mice's ear was described similarly in these studies.

However, it is important to note that the scoring of visible inflammatory reactions such as erythema and desquamation performed in this study is subjective and depends on the respective observer. This challenge was met by not varying the observers throughout the observation period. In addition, the ear thickness values obtained with the specially adapted calliper can be seen as a more objective criterion to assess the acute inflammation reaction after the irradiation. It most likely corresponds to the acute inflammatory reactions in the skin, e.g. oedema and hyperaemia (Dombrowsky et al., 2019). The presence of prolonged ear swelling at the end of the observation period of 90 days could thus be a sign of prolonged or chronic inflammation reaction (Dombrowsky et al., 2019).

The results at hand indicate that pMBRT could be a way to improve the therapeutic index of radiation therapy through the combination of the inherent physical advantages of proton beams; i.e. the steep dose fall-off and thus sparing of normal tissue behind the target volume and the reduced dose deposition in front of the target due to distribution in peak and valley doses. The reduction of acute side effects in pMBRT demonstrated by this experiment could not only ameliorate the patients' immediate condition during radiation therapy but also reduce the risk for the so-called consequential late effects.

4.1 Limitations of this study

In this study, side effects following proton Minibeam irradiation were only monitored for 90 days, which shows acute side effects only. While acute side effects of radiation therapy can be dose-limiting in some cases, late side effects like fibrosis or secondary malignancy must not be disregarded. The increased ear thickness observed in the larger beam size groups at the end of the observation period could indicate either prolonged inflammation reaction or induction of fibrosis. Generally, it is important to state that the severity of acute side effects does not necessarily allow to draw conclusions regarding the dimensions of late effects (Dörr W., 2013). However, Dombrowsky et al. were able to show in their work on acute damage and chronic side effects in murine ears after high-dose radiation that increased ear thickness does indeed correlate with the size of fibrotic area and inflammation processes in the skin (Dombrowsky et al., 2019). Hence, the increased ear thickness at the end of the observation period can be used as a predictive criterion for late side effects after irradiation at least to some extent. Regarding pMBRT, this implies an improved tissue sparing effect for the smaller beam sizes not only in terms of acute radiation effects but also regarding long-term adverse effects. In an even longer observation period of six months, Prezado et al. showed reduced side effects in terms of skin and CNS damage in their study on side effects after pMBRT on normal rat brain (Prezado Y. et al., 2017).

Regarding secondary malignancies, further long-term studies will be needed to fully assess the clinical advantages of pMBRT.

As no tumour model was used in this study, no observation regarding tumour control was obtained. However, it was shown in several experiments that due to lateral scattering, irradiation with proton minibeams results in homogeneous irradiation in a certain depth of the irradiated volume defined by the protons' energy (Prezado Y. & Fois, 2013; Sammer, Greubel, Girst, & Dollinger, 2017). Hence, the target volume would be irradiated homogeneously and thus tumour control should be expected in analogy to conventional broad beam irradiation.

Accordingly, more recent studies did indeed show the effectiveness of tumour control through pMBRT in RG2 glioma bearing rats (Prezado Y. et al., 2018). In a comparison of the pMBRT concept and conventional broad beam proton therapy in the same animal model,

a significantly enhanced tumour control was achieved in the pMBRT group while maintaining the reduction of adverse side effects (Prezado Y. et al., 2019).

In this study, protons with an energy of 20 MeV were used to create the proton minibeams. In contrast, in clinical proton radiotherapy, proton energies from around 60 MeV (for eye tumours) up to 160 MeV (for deeper lying tumours) are used (Schulz-Ertner & Debus, 2013). Clinical implementation of pMBRT would, therefore, require much higher energies than those used in this study. However, the physical feasibility of the creation of proton minibeams with an energy of 109 MeV (Dilmanian F.A. et al., 2015) and 100 MeV (Peucelle et al., 2015; Prezado Y. et al., 2017) at existing particle therapy centres has recently been shown. A proton energy of 100 MeV correlates to a range of 77 mm water equivalent (Peucelle et al., 2015) and is clinically relevant as it allows for example for the treatment of a tumour at the centre of a human brain (Prezado Y. et al., 2017). Also, biological studies in a clinical set-up have been carried out at the Orsay Proton therapy Center (Prezado Y. et al., 2017). Here, proton beams with an energy of 100 MeV have been used as well and an average dose of 25 +- 1 Gy was applied in one single fraction (Prezado Y. et al., 2017). This indicates that pMBRT is theoretically feasible at clinically relevant beam energies in existing clinical therapy centres.

Using high LET radiation – especially heavy ions – could be another interesting future application of spatial fractionation with minibeams. In addition to the physical advantage of inverse dose distribution profile of heavy ions similar to protons, high LET radiation offers additional biological advantages and can overcome certain mechanisms of radioresistance such as hypoxia, sublethal damage recovery (SLDR) and dependence on cell cycle (Weber KJ., 2013). Therefore, efficiency in terms of tumour control could be increased while benefitting from the normal tissue protection achieved by spatial fractionation and the inherent favourable depth-dose profile of heavy ions. Of course, further investigations and preclinical studies confirming this hypothesis will be needed.

4.2 Technical challenges

Exact and unchanging patient positioning both during one irradiation session and between the different sessions is one of the key requirements to clinical radiotherapy to ensure precise dose application to the actual tumour. This challenge has been met over the last

decades by improved patient positioning, e.g. employing masks designed individually for the patients, and image-guided therapy strategies. In pMBRT, patient positioning will be even more important not only because of the necessity of calculating the spread-out Bragg Peak exactly around the tumour site for sufficient dose deposition and hence tumour control. Further studies will also be necessary to show whether the normal tissue-sparing effect will decrease in fractionated therapy regimes due to the movement of the actual minibeams. Furthermore, this radiation technique may be even more prone to patients' movements, e.g. caused by respiration and cardiac cycle. Hence, it seems logical that clinical implementation for pMBRT will particularly be successful in tumour sites less affected by this kind of movement, for example in the brain (Peucelle et al., 2015).

Another technical challenge important to mention will be the necessity to account for range uncertainties and/or tissue inhomogeneities in patients as proton beams are more susceptible to changes in tissue constitution (Dörr W. & Joiner, 2010). Although this problem is similar in conventional broad beam proton radiotherapy, it appears to be even more prominent because of the requirement to calculate not only the beams' range but also their lateral scattering. In the present study, this was negligible as the mice's ears are rather thin and the effects on the proton beam easier to evaluate. However, for the clinical implementation of pMBRT, this challenge will have to be considered.

4.3 Possible indications for clinical application of pMBRT

Current indications for conventional proton radiation therapy have already been stated above (cf. chapter 1.2.3). Conventional broad beam proton radiation therapy is mainly used in tumours which are adjacent to critical tissues, for example, CNS tumours, head and neck tumours and craniopharyngiomas of the skull base (Schulz-Ertner & Debus, 2013). Also, it is employed in paediatric oncology with the aim to reduce the risk of secondary malignancies by reducing the dose applied to normal tissue (Schulz-Ertner & Debus, 2013).

The beneficial effects of broad beam proton irradiation are mainly due to the sharp dose fall-off distal to the target volume. Irradiation with proton minibeams as investigated in this work could offer the opportunity to further reduce the damage to normal tissue, especially in the entrance channel in front of the target volume. This is most important when administering radiation therapy to tumours in proximity to radiosensitive tissues, e.g. in the brain. By means of minibeam irradiation, the dose applied to normal tissue both in front

of and distal to the target volume is redistributed differently, which results in smaller adverse side effects after the irradiation. In 2017, Prezado et al. compared pMBRT to conventional broad beam therapy with protons at a clinically relevant energy of 100 MeV (Prezado Y. et al., 2017). While they observed severe adverse effects in the broad beam therapy group, their results showed no skin damage and, even more importantly, significantly fewer CNS side effects in the pMBRT group (Prezado Y. et al., 2017). This supports the idea of applying pMBRT especially to CNS tumours, which has been proposed earlier due to the relative stability of the head region concerning respiratory and cardiovascular movement (Peucelle et al., 2015).

Another indication for pMBRT could be head and neck tumours, where mucositis enoralis is an acute radiation side effect that can be dose-limiting and hence impair sufficient treatment (Dörr W., 2013). Of course, tissue inhomogeneities in the head and neck region have to be considered in the calculation of the proton minibeams as explained above. This could prevent an optimal exploitation of pMBRT in the treatment of head and neck tumours. However, the reduction of acute side effects of pMBRT shown in this work alongside other studies renders pMBRT a possible future therapeutic approach in treatment settings where acute side effects are dose-limiting.

In paediatric oncology, randomized controlled trials to prove the superiority of radiation therapy with protons over conventional therapy with photons are not available. Still, recent reviews regarding the treatment of paediatric CNS tumours do indeed indicate that proton radiation therapy is superior to photon irradiation (Armoogum & Thorp, 2015; Huynh et al., 2019). The benefit for paediatric patients is particularly pronounced in late effects, where an improvement has been found in terms of neurocognitive and endocrine function as well as health-related quality of life (Armoogum & Thorp, 2015; Huynh et al., 2019). The results at hand indicate a significant reduction of acute side effects after irradiation with proton minibeams. Also, more recent studies have shown reduced side effects also after long-term observation, which makes pMBRT a promising future therapy approach for paediatric oncology due to further reduction of expected side effects.

Another important late effect of radiotherapy both in children and adult patients is the development of secondary malignancies induced by radiation. For adults, this risk is about 1% after conventional radiation therapy with photons (Trott K.R., 2017), but it is important

to note that the risk of recurrence of the primary malignancy is much more relevant clinically (Trott K.R., 2010). In contrast, it is much more likely for the younger paediatric patients to experience secondary tumours due to their expected longer life span (Trott K.R., 2010). A reduction of this risk through radiotherapy with protons would hence be of great importance. While some authors state that it should theoretically be lower for proton irradiation (Dörr W. & Joiner, 2010), others claim that at least it should not be higher for particle therapy (Trott K.R., 2017). Indeed, some studies indicate a significantly lower risk of developing secondary cancers after radiotherapy with protons than following radiation therapy with photons (Chung, Keating, Yock, & Tarbell, 2008). As pMBRT aims to confine most of the dose to the actual tumour and to deposit less dose in normal tissue, it is likely to further reduce the risk of secondary cancers. Of course, this will have to be further investigated in future long-term studies. It is important to note that most radiation-induced secondary tumours develop in the high dose volume (Trott K.R., 2010). Thus, it would be interesting to evaluate if the beam channels in spatially fractionated irradiation are at higher risk for secondary malignancies. However, due to the very high dose in the beam channels, surviving tumour stem cells within the beam channel seem to be very unlikely.

In conventional modern radiation therapy, standard therapeutic schemes usually involve 5 fractions per week with around 2 Gy per fraction, resulting in a total dose of around 60 Gy (Weber KJ., 2013). This fractionated therapy regime aims primarily at enhancing sublethal damage recovery (SLDR) and hence improving the toleration of therapy (Weber KJ., 2013). The intervals between the respective fraction are generally chosen to be greater than or equal to at least 6 hours to spare normal tissue to allow for SLDR especially in normal tissues (Weber KJ., 2013). Due to its ability to enhance normal tissue sparing, especially in front of the target, pMBRT could offer a way of dose escalation while maintaining the tissue damage on a tolerable level. It could hence also be used to enable faster, hypofractionated therapy schemes, similar to high LET radiation (Dilmanian F.A. et al., 2015; Weber KJ., 2013). Another possible indication could be very radioresistant tumours with side effects being kept tolerable while performing a dose escalation to the tumour (Peucelle et al., 2015; Prezado Y. et al., 2017).

Furthermore, the reduced damage to normal tissue could make pMBRT a novel therapeutic approach in stereotactic radiosurgery. Current indications for radiosurgery include brain metastases, where local control rates have been shown to depend directly on the dose

applied (Zabel-du Bois A., Debus J., 2013). Here, a substantial dose escalation could be achieved through pMBRT while keeping adverse side effects on a tolerable level similar to conventional existing radiosurgical therapy. In the therapy of cerebral arteriovenous malformations – a benign medical condition that is treated with stereotactic radiosurgery today (Zabel-du Bois A., Debus J., 2013) – pMBRT could allow for a reduction of adverse side effects. Likewise, radiosurgical treatment strategies have been applied to other benign diseases such as trigeminal neuralgia or epilepsy and good results have been obtained (Zabel-du Bois A., Debus J., 2013). pMBRT would allow for a precise dose restriction to the target in question while reducing side effects through normal tissue sparing. For epilepsy, studies indicate good results in terms of reduced seizure activity while maintaining a normal cerebral function after treatment with so-called X-ray microbeams (Romanelli et al., 2013; Serduc et al., 2010). The localisation of the conditions mentioned in the head region renders these illnesses potential future candidates for pMBRT as patients' movements (e.g. due to cardiorespiratory changes) can be controlled more easily than for example in the torso (Peucelle et al., 2015; Prezado Y. et al., 2017).

5. Conclusion

The present results confirm that proton minibeam irradiation spares normal tissue. The smaller beam sizes – as they would occur in shallow parts of the irradiated volume – result in significantly reduced acute side effects. The observed inflammation reaction increases with increasing beam size and the maximum reaction for each beam size group shifts towards later time points. Also, the largest beam sizes result in prolonged swelling of the irradiated ear and incomplete recovery after the observation period of 90 days, which could indicate long-term consequences.

All minibeam beam sizes are superior to homogenous irradiation in terms of inflammation reaction and swelling. This makes Proton Minibeam Radiation Therapy a promising approach that can be used either to reduce early and late side effects in irradiation with equal dose or to enable dose-escalation schemes for radioresistant tumours. Furthermore, the increased therapeutic window due to the enhanced normal tissue sparing could allow for the implementation of so-called hypofractionated therapy regimes in the future.

6. Acknowledgements

First of all, I would like to thank Prof. Dr. Thomas E. Schmid for his patient and unwavering support during the whole MD thesis process and without whom this thesis would definitely not exist.

A big thank you to everyone at the Institute of Innovative Radiotherapy (HMGU) and Department of Radiation Oncology (MRI): Prof. Dr. Combs, Prof. Dr. Wilkens, Prof. Dr. Multhoff, PD Dr. Gehrmann, Dr. Lämmer, Dr. Schilling, Dr. Dobiasch, K. Ilicic, A. Dombrowsky, A. Mair, M. Stein and D. Walsh.

A very big thank you to Matthias Sammer (Universität der Bundeswehr München) for his support and the exceptional collaboration during this work. Thank you to everyone at the Universität der Bundeswehr München, especially Prof. Dr. Günther Dollinger, J. Reindl, Dr. Greubel and C. Siebenwirth.

Thank you to Prof. Dr. Schlegel and C. Grubmüller at the Institute of Neuropathology (MRI).

Thank you to Dr. Steiger from the Institute of Pathology (MRI).

Thank you to the Institut für Medizinische Informatik, Statistik und Epidemiologie, especially Armin Ott, for providing me with the necessary knowledge to perform the statistical evaluation.

Thank you to my family and all my friends, who had to endure my complaining about the various problems encountered on the way and who kept me going. Thank you to J.A. for eliminating many blank spaces.

7. Appendix

7.1 List of figures

7.2 List of tables

7.3 Statistical evaluation data

One-way ANOVA for repeated measures with LSD test: Right ear thickness per beam size group over the observation period

Multiple Comparisons

Maß: MEASURE_1

LSD

(I)group		Mittlere Differenz (I-J)	Standard Fehler	Sig.	95%-Konfidenzintervall Untergrenze	95%-Konfidenzintervall Obergrenze
sham	90 µm	-7,7917	14,12831	0,584	-36,1836	20,6002
	200 µm	-33,2292*	14,12831	0,023	-61,6211	-4,8373
	310 µm	-52,0833*	14,12831	0,001	-80,4752	-23,6914
	450 µm	-86,8750*	14,12831	0,000	-115,2669	-58,4831
	560 µm	-119,5694*	14,12831	0,000	-147,9613	-91,1775
	900 µm	-151,9111*	14,12831	0,000	-180,3030	-123,5192
90 µm	sham	7,7917	14,12831	0,584	-20,6002	36,1836
	200 µm	-25,4375	14,12831	0,078	-53,8294	2,9544
	310 µm	-44,2917*	14,12831	0,003	-72,6836	-15,8998
	450 µm	-79,0833*	14,12831	0,000	-107,4752	-50,6914
	560 µm	-111,7778*	14,12831	0,000	-140,1697	-83,3859
	900 µm	-144,1194*	14,12831	0,000	-172,5113	-115,7275
200 µm	sham	33,2292*	14,12831	0,023	4,8373	61,6211
	90 µm	25,4375	14,12831	0,078	-2,9544	53,8294
	310 µm	-18,8542	14,12831	0,188	-47,2461	9,5377
	450 µm	-53,6458*	14,12831	0,000	-82,0377	-25,2539
	560 µm	-86,3403*	14,12831	0,000	-114,7322	-57,9484
	900 µm	-118,6819*	14,12831	0,000	-147,0738	-90,2900
310 µm	sham	52,0833*	14,12831	0,001	23,6914	80,4752
	90 µm	44,2917*	14,12831	0,003	15,8998	72,6836
	200 µm	18,8542	14,12831	0,188	-9,5377	47,2461
	450 µm	-34,7917*	14,12831	0,017	-63,1836	-6,3998
	560 µm	-67,4861*	14,12831	0,000	-95,8780	-39,0942
	900 µm	-99,8278*	14,12831	0,000	-128,2197	-71,4359
450 µm	sham	86,8750*	14,12831	0,000	58,4831	115,2669
	90 µm	79,0833*	14,12831	0,000	50,6914	107,4752
	200 µm	53,6458*	14,12831	0,000	25,2539	82,0377
	310 µm	34,7917*	14,12831	0,017	6,3998	63,1836
	560 µm	-32,6944*	14,12831	0,025	-61,0863	-4,3025
	900 µm	-65,0361*	14,12831	0,000	-93,4280	-36,6442
560 µm	sham	119,5694*	14,12831	0,000	91,1775	147,9613
	90 µm	111,7778*	14,12831	0,000	83,3859	140,1697
	200 µm	86,3403*	14,12831	0,000	57,9484	114,7322
	310 µm	67,4861*	14,12831	0,000	39,0942	95,8780
	450 µm	32,6944*	14,12831	0,025	4,3025	61,0863
	900 µm	-32,3417*	14,12831	0,026	-60,7336	-3,9498
900 µm	sham	151,9111*	14,12831	0,000	123,5192	180,3030
	90 µm	144,1194*	14,12831	0,000	115,7275	172,5113
	200 µm	118,6819*	14,12831	0,000	90,2900	147,0738
	310 µm	99,8278*	14,12831	0,000	71,4359	128,2197
	450 µm	65,0361*	14,12831	0,000	36,6442	93,4280
	560 µm	32,3417*	14,12831	0,026	3,9498	60,7336

Grundlage: beobachtete Mittelwerte.

Der Fehlerterm ist Mittel der Quadrate(Fehler) = 798,437.

*. Die mittlere Differenz ist auf dem ,05-Niveau signifikant.

One-way ANOVA for repeated measures with LSD test: Change in right ear thickness per beam size group over the observation period

Multiple Comparisons

Maß: MEASURE_1

LSD

(I)group		Mittlere Differenz (I-J)	Standard Fehler	Sig.	95%-Konfidenzintervall Untergrenze	95%-Konfidenzintervall Obergrenze
sham	90 µm	-7,7917	14,67147	0,598	-37,2751	21,6918
	200 µm	-34,6875*	14,67147	0,022	-64,1709	-5,2041
	310 µm	-52,5000*	14,67147	0,001	-81,9834	-23,0166
	450 µm	-87,0833*	14,67147	0,000	-116,5668	-57,5999
	560 µm	-117,2778*	14,67147	0,000	-146,7612	-87,7943
	900 µm	-157,7444*	14,67147	0,000	-187,2279	-128,2610
90 µm	sham	7,7917	14,67147	0,598	-21,6918	37,2751
	200 µm	-26,8958	14,67147	0,073	-56,3793	2,5876
	310 µm	-44,7083*	14,67147	0,004	-74,1918	-15,2249
	450 µm	-79,2917*	14,67147	0,000	-108,7751	-49,8082
	560 µm	-109,4861*	14,67147	0,000	-138,9695	-80,0027
	900 µm	-149,9528*	14,67147	0,000	-179,4362	-120,4693
200 µm	sham	34,6875*	14,67147	0,022	5,2041	64,1709
	90 µm	26,8958	14,67147	0,073	-2,5876	56,3793
	310 µm	-17,8125	14,67147	0,231	-47,2959	11,6709
	450 µm	-52,3958*	14,67147	0,001	-81,8793	-22,9124
	560 µm	-82,5903*	14,67147	0,000	-112,0737	-53,1068
	900 µm	-123,0569*	14,67147	0,000	-152,5404	-93,5735
310 µm	sham	52,5000*	14,67147	0,001	23,0166	81,9834
	90 µm	44,7083*	14,67147	0,004	15,2249	74,1918
	200 µm	17,8125	14,67147	0,231	-11,6709	47,2959
	450 µm	-34,5833*	14,67147	0,022	-64,0668	-5,0999
	560 µm	-64,7778*	14,67147	0,000	-94,2612	-35,2943
	900 µm	-105,2444*	14,67147	0,000	-134,7279	-75,7610
450 µm	sham	87,0833*	14,67147	0,000	57,5999	116,5668
	90 µm	79,2917*	14,67147	0,000	49,8082	108,7751
	200 µm	52,3958*	14,67147	0,001	22,9124	81,8793
	310 µm	34,5833*	14,67147	0,022	5,0999	64,0668
	560 µm	-30,1944*	14,67147	0,045	-59,6779	-0,7110
	900 µm	-70,6611*	14,67147	0,000	-100,1445	-41,1777
560 µm	sham	117,2778*	14,67147	0,000	87,7943	146,7612
	90 µm	109,4861*	14,67147	0,000	80,0027	138,9695
	200 µm	82,5903*	14,67147	0,000	53,1068	112,0737
	310 µm	64,7778*	14,67147	0,000	35,2943	94,2612
	450 µm	30,1944*	14,67147	0,045	0,7110	59,6779
	900 µm	-40,4667*	14,67147	0,008	-69,9501	-10,9832
900 µm	sham	157,7444*	14,67147	0,000	128,2610	187,2279
	90 µm	149,9528*	14,67147	0,000	120,4693	179,4362
	200 µm	123,0569*	14,67147	0,000	93,5735	152,5404
	310 µm	105,2444*	14,67147	0,000	75,7610	134,7279
	450 µm	70,6611*	14,67147	0,000	41,1777	100,1445
	560 µm	40,4667*	14,67147	0,008	10,9832	69,9501

Grundlage: beobachtete Mittelwerte.
Der Fehlerterm ist Mittel der Quadrate(Fehler) = 861,009.

*. Die mittlere Differenz ist auf dem ,05-Niveau signifikant.

One-way ANOVA with LSD test: Maximum increase in right ear thickness per beam size group

Multiple Comparisons

Abhängige Variable:	Maximum Change in Ear					
LSD						
					95%-Konfidenzintervall	
(I)group		Mittlere Differenz (I-J)	Standard Fehler	Sig.	Untergrenze	Obergrenze
sham	90 µm	-8,9583	36,06350	0,805	-81,4306	63,5140
	200 µm	-69,7917	36,06350	0,059	-142,2640	2,6806
	310 µm	-131,2500*	36,06350	0,001	-203,7223	-58,7777
	450 µm	-184,1667*	36,06350	0,000	-256,6390	-111,6944
	560 µm	-307,2917*	36,06350	0,000	-379,7640	-234,8194
	900 µm	-437,2917*	36,06350	0,000	-509,7640	-364,8194
90 µm	sham	8,9583	36,06350	0,805	-63,5140	81,4306
	200 µm	-60,8333	36,06350	0,098	-133,3056	11,6390
	310 µm	-122,2917*	36,06350	0,001	-194,7640	-49,8194
	450 µm	-175,2083*	36,06350	0,000	-247,6806	-102,7360
	560 µm	-298,3333*	36,06350	0,000	-370,8056	-225,8610
	900 µm	-428,3333*	36,06350	0,000	-500,8056	-355,8610
200 µm	sham	69,7917	36,06350	0,059	-2,6806	142,2640
	90 µm	60,8333	36,06350	0,098	-11,6390	133,3056
	310 µm	-61,4583	36,06350	0,095	-133,9306	11,0140
	450 µm	-114,3750*	36,06350	0,003	-186,8473	-41,9027
	560 µm	-237,5000*	36,06350	0,000	-309,9723	-165,0277
	900 µm	-367,5000*	36,06350	0,000	-439,9723	-295,0277
310 µm	sham	131,2500*	36,06350	0,001	58,7777	203,7223
	90 µm	122,2917*	36,06350	0,001	49,8194	194,7640
	200 µm	61,4583	36,06350	0,095	-11,0140	133,9306
	450 µm	-52,9167	36,06350	0,149	-125,3890	19,5556
	560 µm	-176,0417*	36,06350	0,000	-248,5140	-103,5694
	900 µm	-306,0417*	36,06350	0,000	-378,5140	-233,5694
450 µm	sham	184,1667*	36,06350	0,000	111,6944	256,6390
	90 µm	175,2083*	36,06350	0,000	102,7360	247,6806
	200 µm	114,3750*	36,06350	0,003	41,9027	186,8473
	310 µm	52,9167	36,06350	0,149	-19,5556	125,3890
	560 µm	-123,1250*	36,06350	0,001	-195,5973	-50,6527
	900 µm	-253,1250*	36,06350	0,000	-325,5973	-180,6527
560 µm	sham	307,2917*	36,06350	0,000	234,8194	379,7640
	90 µm	298,3333*	36,06350	0,000	225,8610	370,8056
	200 µm	237,5000*	36,06350	0,000	165,0277	309,9723
	310 µm	176,0417*	36,06350	0,000	103,5694	248,5140
	450 µm	123,1250*	36,06350	0,001	50,6527	195,5973
	900 µm	-130,0000*	36,06350	0,001	-202,4723	-57,5277
900 µm	sham	437,2917*	36,06350	0,000	364,8194	509,7640
	90 µm	428,3333*	36,06350	0,000	355,8610	500,8056
	200 µm	367,5000*	36,06350	0,000	295,0277	439,9723
	310 µm	306,0417*	36,06350	0,000	233,5694	378,5140
	450 µm	253,1250*	36,06350	0,000	180,6527	325,5973
	560 µm	130,0000*	36,06350	0,001	57,5277	202,4723

Grundlage: beobachtete Mittelwerte.
Der Fehlerterm ist Mittel der Quadrate(Fehler) = 5202,303.
*. Die mittlere Differenz ist auf dem 0,05-Niveau signifikant.

Pearson's correlation coefficient: Association between maximum ear thickness and beam size group

Korrelationen			
		beam size	thickness (tmax)
beam size	Korrelation nach Pearson	1	,984**
	Signifikanz (2-seitig)		0,000
	N	7	7
thickness (tmax)	Korrelation nach Pearson	,984**	1
	Signifikanz (2-seitig)	0,000	
	N	7	7

**. Die Korrelation ist auf dem Niveau von 0,01 (2-seitig) signifikant.

Pearson's correlation coefficient: Association between maximum increase in right ear thickness and beam size group

Korrelationen			
		Beam Size	Maximum increase in Right Ear Thickness
Beam Size	Korrelation nach Pearson	1	,986**
	Signifikanz (2-seitig)		0,000
	N	7	7
Maximum increase in Right Ear Thickness	Korrelation nach Pearson	,986**	1
	Signifikanz (2-seitig)	0,000	
	N	7	7

**. Die Korrelation ist auf dem Niveau von 0,01 (2-seitig) signifikant.

Pearson's correlation coefficient: Association between change in right ear thickness at the end of observation period and beam size group

Korrelationen			
		Beam Size	Change in Right Ear Thickness at the end of observation
Beam Size	Korrelation nach Pearson	1	,930**
	Signifikanz (2-seitig)		0,002
	N	7	7
Change in Right Ear Thickness at the end of observation	Korrelation nach Pearson	,930**	1
	Signifikanz (2-seitig)	0,002	
	N	7	7

**. Die Korrelation ist auf dem Niveau von 0,01 (2-seitig) signifikant.

One-way ANOVA with Greenhouse-Geisser correction and LSD test: Right ear thickness at the end of the observation period

ONEWAY deskriptive Statistiken

Mean Thickness (tend)

	N	Mittelwert	Std.-Abweichung	Std.-Fehler	95%-Konfidenzintervall für den Mittelwert		Minimum	Maximum
					Untergrenze	Obergrenze		
sham	8	212,5833	5,58555	1,97479	207,9137	217,2530	208,33	224,67
90 µm	8	211,2500	5,16321	1,82547	206,9334	215,5666	205,00	220,00
200 µm	8	224,1667	11,31511	4,00050	214,7070	233,6263	215,33	248,67
310 µm	8	227,7917	16,57588	5,86046	213,9339	241,6495	211,67	263,33
450 µm	8	247,3750	58,49934	20,68264	198,4683	296,2817	221,67	392,00
560 µm	8	242,9583	24,50490	8,66379	222,4717	263,4449	215,00	294,67
900 µm	8	247,0000	17,25624	6,10100	232,5734	261,4266	228,67	271,33
Gesamt	56	230,4464	28,62846	3,82564	222,7797	238,1132	205,00	392,00

Einfaktorielle ANOVA

Mean Thickness (tend)

	Quadratsumme	df	Mittel der Quadrate	F	Signifikanz
Zwischen den Gruppen	11609,770	6	1934,962	2,833	0,019
Innerhalb der Gruppen	33467,625	49	683,013		
Gesamt	45077,395	55			

Post-Hoc-Tests

Mehrfachvergleiche

Abhängige Variable: Mean Thickness (tend)

LSD

(I) group		Mittlere Differenz (I-J)	Std.-Fehler	Signifikanz	95%-Konfidenzintervall	
					Untergrenze	Obergrenze
sham	90 µm	1,33333	13,06726	0,919	-24,9263	27,5930
	200 µm	-11,58333	13,06726	0,380	-37,8430	14,6763
	310 µm	-15,20833	13,06726	0,250	-41,4680	11,0513
	450 µm	-34,79167*	13,06726	0,010	-61,0513	-8,5320
	560 µm	-30,37500*	13,06726	0,024	-56,6346	-4,1154
	900 µm	-34,41667*	13,06726	0,011	-60,6763	-8,1570
90 µm	sham	-1,33333	13,06726	0,919	-27,5930	24,9263
	200 µm	-12,91667	13,06726	0,328	-39,1763	13,3430
	310 µm	-16,54167	13,06726	0,212	-42,8013	9,7180
	450 µm	-36,12500*	13,06726	0,008	-62,3846	-9,8654
	560 µm	-31,70833*	13,06726	0,019	-57,9680	-5,4487
	900 µm	-35,75000*	13,06726	0,009	-62,0096	-9,4904
200 µm	sham	11,58333	13,06726	0,380	-14,6763	37,8430
	90 µm	12,91667	13,06726	0,328	-13,3430	39,1763
	310 µm	-3,62500	13,06726	0,783	-29,8846	22,6346
	450 µm	-23,20833	13,06726	0,082	-49,4680	3,0513
	560 µm	-18,79167	13,06726	0,157	-45,0513	7,4680
	900 µm	-22,83333	13,06726	0,087	-49,0930	3,4263
310 µm	sham	15,20833	13,06726	0,250	-11,0513	41,4680
	90 µm	16,54167	13,06726	0,212	-9,7180	42,8013
	200 µm	3,62500	13,06726	0,783	-22,6346	29,8846
	450 µm	-19,58333	13,06726	0,140	-45,8430	6,6763
	560 µm	-15,16667	13,06726	0,251	-41,4263	11,0930
	900 µm	-19,20833	13,06726	0,148	-45,4680	7,0513
450 µm	sham	34,79167*	13,06726	0,010	8,5320	61,0513
	90 µm	36,12500*	13,06726	0,008	9,8654	62,3846
	200 µm	23,20833	13,06726	0,082	-3,0513	49,4680
	310 µm	19,58333	13,06726	0,140	-6,6763	45,8430
	560 µm	4,41667	13,06726	0,737	-21,8430	30,6763
	900 µm	0,37500	13,06726	0,977	-25,8846	26,6346
560 µm	sham	30,37500*	13,06726	0,024	4,1154	56,6346
	90 µm	31,70833*	13,06726	0,019	5,4487	57,9680
	200 µm	18,79167	13,06726	0,157	-7,4680	45,0513
	310 µm	15,16667	13,06726	0,251	-11,0930	41,4263
	450 µm	-4,41667	13,06726	0,737	-30,6763	21,8430
	900 µm	-4,04167	13,06726	0,758	-30,3013	22,2180
900 µm	sham	34,41667*	13,06726	0,011	8,1570	60,6763
	90 µm	35,75000*	13,06726	0,009	9,4904	62,0096
	200 µm	22,83333	13,06726	0,087	-3,4263	49,0930
	310 µm	19,20833	13,06726	0,148	-7,0513	45,4680
	450 µm	-0,37500	13,06726	0,977	-26,6346	25,8846
	560 µm	4,04167	13,06726	0,758	-22,2180	30,3013

*. Die Differenz der Mittelwerte ist auf dem Niveau 0.05 signifikant.

One-way ANOVA with LSD test: Changes in Right ear thickness at the end of the observation period

Multiple Comparisons

Abhängige Variable: LSD	Change in Ear Thickness at the end of the observation					
					95%-Konfidenzintervall	
(I)group		Mittlere Differenz (I-J)	Standard Fehler	Sig.	Untergrenze	Obergrenze
sham	90 µm	1,3333	14,09304	0,925	-26,9877	29,6544
	200 µm	-13,0417	14,09304	0,359	-41,3627	15,2794
	310 µm	-15,6250	14,09304	0,273	-43,9460	12,6960
	450 µm	-35,0000*	14,09304	0,016	-63,3210	-6,6790
	560 µm	-28,0833	14,09304	0,052	-56,4044	0,2377
	900 µm	-40,2500*	14,09304	0,006	-68,5710	-11,9290
90 µm	sham	-1,3333	14,09304	0,925	-29,6544	26,9877
	200 µm	-14,3750	14,09304	0,313	-42,6960	13,9460
	310 µm	-16,9583	14,09304	0,235	-45,2794	11,3627
	450 µm	-36,3333*	14,09304	0,013	-64,6544	-8,0123
	560 µm	-29,4167*	14,09304	0,042	-57,7377	-1,0956
	900 µm	-41,5833*	14,09304	0,005	-69,9044	-13,2623
200 µm	sham	13,0417	14,09304	0,359	-15,2794	41,3627
	90 µm	14,3750	14,09304	0,313	-13,9460	42,6960
	310 µm	-2,5833	14,09304	0,855	-30,9044	25,7377
	450 µm	-21,9583	14,09304	0,126	-50,2794	6,3627
	560 µm	-15,0417	14,09304	0,291	-43,3627	13,2794
	900 µm	-27,2083	14,09304	0,059	-55,5294	1,1127
310 µm	sham	15,6250	14,09304	0,273	-12,6960	43,9460
	90 µm	16,9583	14,09304	0,235	-11,3627	45,2794
	200 µm	2,5833	14,09304	0,855	-25,7377	30,9044
	450 µm	-19,3750	14,09304	0,175	-47,6960	8,9460
	560 µm	-12,4583	14,09304	0,381	-40,7794	15,8627
	900 µm	-24,6250	14,09304	0,087	-52,9460	3,6960
450 µm	sham	35,0000*	14,09304	0,016	6,6790	63,3210
	90 µm	36,3333*	14,09304	0,013	8,0123	64,6544
	200 µm	21,9583	14,09304	0,126	-6,3627	50,2794
	310 µm	19,3750	14,09304	0,175	-8,9460	47,6960
	560 µm	6,9167	14,09304	0,626	-21,4044	35,2377
	900 µm	-5,2500	14,09304	0,711	-33,5710	23,0710
560 µm	sham	28,0833	14,09304	0,052	-0,2377	56,4044
	90 µm	29,4167*	14,09304	0,042	1,0956	57,7377
	200 µm	15,0417	14,09304	0,291	-13,2794	43,3627
	310 µm	12,4583	14,09304	0,381	-15,8627	40,7794
	450 µm	-6,9167	14,09304	0,626	-35,2377	21,4044
	900 µm	-12,1667	14,09304	0,392	-40,4877	16,1544
900 µm	sham	40,2500*	14,09304	0,006	11,9290	68,5710
	90 µm	41,5833*	14,09304	0,005	13,2623	69,9044
	200 µm	27,2083	14,09304	0,059	-1,1127	55,5294
	310 µm	24,6250	14,09304	0,087	-3,6960	52,9460
	450 µm	5,2500	14,09304	0,711	-23,0710	33,5710
	560 µm	12,1667	14,09304	0,392	-16,1544	40,4877

Grundlage: beobachtete Mittelwerte.
Der Fehlerterm ist Mittel der Quadrate(Fehler) = 794,455.

*. Die mittlere Differenz ist auf dem 0,05-Niveau signifikant.

One-way ANOVA for repeated measures and LSD test: Inflammation score between beam size groups

Multiple Comparisons

Maß: MEASURE_1

LSD

(I)µm		Mittlere Differenz (I-J)	Standard Fehler	Sig.	95%-Konfidenzintervall Untergrenze	95%-Konfidenzintervall Obergrenze
0	90	-0,0021	0,14020	0,988	-0,2838	0,2797
	200	-0,1063	0,14020	0,452	-0,3880	0,1755
	310	-,3104*	0,14020	0,032	-0,5922	-0,0287
	450	-,6812*	0,14020	0,000	-0,9630	-0,3995
	560	-1,2375*	0,14020	0,000	-1,5192	-0,9558
	900	-1,5417*	0,14020	0,000	-1,8234	-1,2599
90	0	0,0021	0,14020	0,988	-0,2797	0,2838
	200	-0,1042	0,14020	0,461	-0,3859	0,1776
	310	-,3083*	0,14020	0,033	-0,5901	-0,0266
	450	-,6792*	0,14020	0,000	-0,9609	-0,3974
	560	-1,2354*	0,14020	0,000	-1,5172	-0,9537
	900	-1,5396*	0,14020	0,000	-1,8213	-1,2578
200	0	0,1063	0,14020	0,452	-0,1755	0,3880
	90	0,1042	0,14020	0,461	-0,1776	0,3859
	310	-0,2042	0,14020	0,152	-0,4859	0,0776
	450	-,5750*	0,14020	0,000	-0,8567	-0,2933
	560	-1,1313*	0,14020	0,000	-1,4130	-0,8495
	900	-1,4354*	0,14020	0,000	-1,7172	-1,1537
310	0	,3104*	0,14020	0,032	0,0287	0,5922
	90	,3083*	0,14020	0,033	0,0266	0,5901
	200	0,2042	0,14020	0,152	-0,0776	0,4859
	450	-,3708*	0,14020	0,011	-0,6526	-0,0891
	560	-,9271*	0,14020	0,000	-1,2088	-0,6453
	900	-1,2313*	0,14020	0,000	-1,5130	-0,9495
450	0	,6812*	0,14020	0,000	0,3995	0,9630
	90	,6792*	0,14020	0,000	0,3974	0,9609
	200	,5750*	0,14020	0,000	0,2933	0,8567
	310	,3708*	0,14020	0,011	0,0891	0,6526
	560	-,5563*	0,14020	0,000	-0,8380	-0,2745
	900	-,8604*	0,14020	0,000	-1,1422	-0,5787
560	0	1,2375*	0,14020	0,000	0,9558	1,5192
	90	1,2354*	0,14020	0,000	0,9537	1,5172
	200	1,1313*	0,14020	0,000	0,8495	1,4130
	310	,9271*	0,14020	0,000	0,6453	1,2088
	450	,5563*	0,14020	0,000	0,2745	0,8380
	900	-,3042*	0,14020	0,035	-0,5859	-0,0224
900	0	1,5417*	0,14020	0,000	1,2599	1,8234
	90	1,5396*	0,14020	0,000	1,2578	1,8213
	200	1,4354*	0,14020	0,000	1,1537	1,7172
	310	1,2313*	0,14020	0,000	0,9495	1,5130
	450	,8604*	0,14020	0,000	0,5787	1,1422
	560	,3042*	0,14020	0,035	0,0224	0,5859

Grundlage: beobachtete Mittelwerte.
Der Fehlerterm ist Mittel der Quadrate(Fehler) = ,079.

*. Die mittlere Differenz ist auf dem ,05-Niveau signifikant.

Pearson’s correlation coefficient: Association between maximum score and beam size group

Korrelationen

		beam size [µm]	Score maximum
beam size [µm]	Korrelation nach Pearson	1	,931**
	Signifikanz (2-seitig)		0,002
	N	7	7
Score maximum	Korrelation nach Pearson	,931**	1
	Signifikanz (2-seitig)	0,002	
	N	7	7

**. Die Korrelation ist auf dem Niveau von 0,01 (2-seitig) signifikant.

References

Armoogum, K. S., & Thorp, N. (2015). Dosimetric Comparison and Potential for Improved Clinical Outcomes of Paediatric CNS Patients Treated with Protons or IMRT. *Cancers*, *7*(2), 706–722. https://doi.org/10.3390/cancers7020706

Baluchamy, S., Ravichandran, P., Periyakaruppan, A., Ramesh, V., Hall, J. C., Zhang, Y., Jejelowo, O., Gridley, D. S., Wu, H., & Ramesh, G. T. (2010). Induction of cell death through alteration of oxidants and antioxidants in lung epithelial cells exposed to high energy protons. *The Journal of Biological Chemistry*, *285*(32), 24769–24774. https://doi.org/10.1074/jbc.M110.138099

Baluchamy, S., Ravichandran, P., Ramesh, V., He, Z., Zhang, Y., Hall, J. C., Jejelowo, O., Gridley, D. S., Wu, H., & Ramesh, G. T. (2012). Reactive oxygen species mediated tissue damage in high energy proton irradiated mouse brain. *Molecular and Cellular Biochemistry*, *360*(1-2), 189–195. https://doi.org/10.1007/s11010-011-1056-2

Bräuer-Krisch, E. [E.], Bravin, A. [A.], Lerch, M., Rosenfeld, A., Stepanek, J., Di Michiel, M., & Laissue, J. A. (2003). Mosfet dosimetry for microbeam radiation therapy at the European Synchrotron Radiation Facility. *Medical Physics*, *30*(4), 583–589. https://doi.org/10.1118/1.1562169

Bräuer-Krisch, E. [E.], Requardt, H. [H.], Régnard, P., Corde, S., Siegbahn, E. [E.], LeDuc, G., Brochard, T. [T.], Blattmann, H., Laissue, J., & Bravin, A. [A.] (2005). New irradiation geometry for microbeam radiation therapy. *Physics in Medicine and Biology*, *50*(13), 3103–3111. https://doi.org/10.1088/0031-9155/50/13/009

Calugaru, V., Nauraye, C. [Catherine], Noël, G., Giocanti, N., Favaudon, V., & Mégnin-Chanet, F. (2011). Radiobiological characterization of two therapeutic proton beams with different initial energy spectra used at the Institut Curie Proton Therapy Center in Orsay. *International Journal of Radiation Oncology, Biology, Physics*, *81*(4), 1136–1143. https://doi.org/10.1016/j.ijrobp.2010.09.003

Chang, J. Y., Zhang, X., Vassiliev, O., Gillin, M., & Mohan, R. (2010). Proton Therapy Targets Cancer Stem Cells in Treatment-resistant Non-small Cell Lung Cancer. *International Journal of Radiation Oncology*Biology*Physics*, *78*(3), S644. https://doi.org/10.1016/j.ijrobp.2010.07.1499

Chung, C. S., Keating, N., Yock, T., & Tarbell, N. (2008). Comparative Analysis of Second Malignancy Risk in Patients Treated with Proton Therapy versus Conventional Photon Therapy. *International Journal of Radiation Oncology*Biology*Physics*, *72*(1), S8. https://doi.org/10.1016/j.ijrobp.2008.06.785

Cox, J. D., Stetz, J., & Pajak, T. F. (1995). Toxicity criteria of the Radiation Therapy Oncology Group (RTOG) and the European organization for research and treatment of cancer (EORTC). *International Journal of Radiation Oncology*Biology*Physics*, *31*(5), 1341–1346. https://doi.org/10.1016/0360-3016(95)00060-C

Dilmanian, F. A. [F. A.] (2002). Response of rat intracranial 9L gliosarcoma to microbeam radiation therapy. *Neuro-Oncology*, *4*(1), 26–38. https://doi.org/10.1215/15228517-4-1-26

Dilmanian, F. A. [F. Avraham], Eley, J. G., & Krishnan, S. (2015). Minibeam therapy with protons and light ions: Physical feasibility and potential to reduce radiation side effects and to facilitate hypofractionation. *International Journal of Radiation Oncology, Biology, Physics*, *92*(2), 469–474. https://doi.org/10.1016/j.ijrobp.2015.01.018

Dilmanian, F. A. [F. Avraham], Qu, Y., Feinendegen, L. E., Peña, L. A., Bacarian, T., Henn, F. A., Kalef-Ezra, J., Liu, S., Zhong, Z., & McDonald, J. W. (2007). Tissue-sparing effect of x-ray microplanar beams particularly in the CNS: Is a bystander effect involved? *Experimental Hematology*, *35*(4 Suppl 1), 69–77. https://doi.org/10.1016/j.exphem.2007.01.014

Dilmanian, F. A. [F. Avraham], Rusek, A., Fois, G. R., Olschowka, J., Desnoyers, N. R., Park, J. Y., Dioszegi, I., Dane, B., Wang, R., Tomasi, D., Lee, H., Hurley, S. d., Coyle, P. K., Meek, A. G., & O'Banion, M. K. (2012). Interleaved Carbon Minibeams: An Experimental Radiosurgery Method With Clinical Potential. *International Journal of Radiation Oncology*Biology*Physics*, *84*(2), 514–519. https://doi.org/10.1016/j.ijrobp.2011.12.025

Dombrowsky, A. C., Schauer, J., Sammer, M., Blutke, A., Walsh, D. W. M., Schwarz, B., Bartzsch, S., Feuchtinger, A., Reindl, J., Combs, S. E., Dollinger, G. [Günther], & Schmid, T. E. (2019). Acute Skin Damage and Late Radiation-Induced Fibrosis and Inflammation in Murine Ears after High-Dose Irradiation. *Cancers*, *11*(5). https://doi.org/10.3390/cancers11050727

Dörr, W. [W.] (2010). Pathogenesis of normal-tissue side-effects. In M. C. Joiner & van der Kogel, A. J. (Eds.), *Basic clinical radiobiology* (4th ed., pp. 169–190). London: Hodder Arnold.

Dörr, W. [W.] (2013). Strahlenpathologie. In Wannenmacher M., Wenz F., Debus J. (Ed.), *Strahlentherapie* (2nd ed., pp. 87–98). Berlin: Springer.

Dörr, W. [W.], & Joiner, M. C. (2010). Protons and other ions in radiotherapy. In M. C. Joiner & van der Kogel, A. J. (Eds.), *Basic clinical radiobiology* (4th ed., pp. 332–338). London: Hodder Arnold.

Dörr, W. [Wolfgang], & Hendry, J. H. (2001). Consequential late effects in normal tissues. *Radiotherapy and Oncology*, *61*(3), 223–231. https://doi.org/10.1016/S0167-8140(01)00429-7

Finnberg, N., Wambi, C., Ware, J. H., Kennedy, A. R., & El-Deiry, W. S. (2008). Gamma-radiation (GR) triggers a unique gene expression profile associated with cell death compared to proton radiation (PR) in mice in vivo. *Cancer Biology & Therapy*, *7*(12), 2023–2033.

Gerelchuluun, A., Hong, Z., Sun, L., Suzuki, K., Terunuma, T., Yasuoka, K., Sakae, T., Moritake, T., & Tsuboi, K. (2011). Induction of in situ DNA double-strand breaks and apoptosis by 200 MeV protons and 10 MV X-rays in human tumour cell lines. *International Journal of Radiation Biology*, *87*(1), 57–70. https://doi.org/10.3109/09553002.2010.518201

Giedzinski, E., Rola, R., Fike, J. R., & Limoli, C. L. (2005). Efficient production of reactive oxygen species in neural precursor cells after exposure to 250 MeV protons. *Radiation Research*, *164*(4 Pt 2), 540–544.

Girdhani, S., Lamont, C., Hahnfeldt, P., Abdollahi, A., & Hlatky, L. (2012). Proton irradiation suppresses angiogenic genes and impairs cell invasion and tumor growth. *Radiation Research*, *178*(1), 33–45.

Girdhani, S., Sachs, R., & Hlatky, L. (2013). Biological effects of proton radiation: What we know and don't know. *Radiation Research*, *179*(3), 257–272. https://doi.org/10.1667/RR2839.1

Girst, S., Greubel, C., Reindl, J., Siebenwirth, C., Zlobinskaya, O., Dollinger, G. [Günther], & Schmid, T. E. (2015). The influence of the channel size on the reduction of side effects in microchannel proton therapy. *Radiation and Environmental Biophysics*, *54*(3), 335–342. https://doi.org/10.1007/s00411-015-0600-y

Girst, S., Greubel, C., Reindl, J., Siebenwirth, C., Zlobinskaya, O., Walsh, D. W. M., Ilicic, K., Aichler, M., Walch, A., Wilkens, J. J., Multhoff, G., Dollinger, G. [Günther], & Schmid, T. E. (2016). Proton Minibeam Radiation Therapy Reduces Side Effects in an In Vivo Mouse Ear Model. *International Journal of Radiation Oncology, Biology, Physics*, *95*(1), 234–241. https://doi.org/10.1016/j.ijrobp.2015.10.020

Goetz, W., Morgan, M. N. M., & Baulch, J. E. (2011). The effect of radiation quality on genomic DNA methylation profiles in irradiated human cell lines. *Radiation Research*, *175*(5), 575–587. https://doi.org/10.1667/RR2390.1

Green, L. M., Murray, D. K., Bant, A. M., Kazarians, G., Moyers, M. F., Nelson, G. A., & Tran, D. T. (2001). Response of thyroid follicular cells to gamma irradiation compared to proton irradiation. I. Initial characterization of DNA damage, micronucleus formation, apoptosis, cell survival, and cell cycle phase redistribution. *Radiation Research*, *155*(1 Pt 1), 32–42.

Greubel, C., Assmann, W., Burgdorf, C., Dollinger, G. [Günther], Du, G., Hable, V., Hapfelmeier, A., Hertenberger, R., Kneschaurek, P., Michalski, D., Molls, M., Reinhardt, S., Röper, B., Schell, S., Schmid, T. E., Siebenwirth, C., Wenzl, T., Zlobinskaya, O., & Wilkens, J. J. (2011). Scanning irradiation device for mice in vivo with pulsed and continuous proton beams. *Radiation and Environmental Biophysics*, *50*(3), 339–344. https://doi.org/10.1007/s00411-011-0365-x

Greubel, C., Hable, V., Drexler, G. A., Hauptner, A. [Andreas], Dietzel, S. [Steffen], Strickfaden, H., Baur, I., Krücken, R. [Reiner], Cremer, T. [Thomas], Friedl, A. A., & Dollinger, G. [Günther] (2008). Quantitative analysis of DNA-damage response factors after sequential ion microirradiation. *Radiation and Environmental Biophysics*, *47*(4), 415–422. https://doi.org/10.1007/s00411-008-0181-0

Hauptner, A. [A.], Dietzel, S. [S.], Drexler, G. A., Reichart, P., Krücken, R. [R.], Cremer, T. [T.], Friedl, A. A., & Dollinger, G. [G.] (2004). Microirradiation of cells with energetic heavy ions. *Radiation and Environmental Biophysics*, *42*(4), 237–245. https://doi.org/10.1007/s00411-003-0222-7

Huynh, M., Marcu, L. G., Giles, E., Short, M., Matthews, D., & Bezak, E. (2019). Are further studies needed to justify the use of proton therapy for paediatric cancers of the central nervous system? A review of current evidence. *Radiotherapy and Oncology*, *133*, 140–148. https://doi.org/10.1016/j.radonc.2019.01.009

Joiner, M. C. (2010). Linear energy transfer and relative biological effectiveness. In M. C. Joiner & van der Kogel, A. J. (Eds.), *Basic clinical radiobiology* (4th ed., pp. 68–77). London: Hodder Arnold.

Köhler, A. (1909). Theorie einer Methode, bisher unmöglich anwendbar hohe Dosen Röntgenstrahlen in der Tiefe des Gewebes zur therapeutischen Wirksamkeit zu bringen ohne schwere Schädigung des Patienten, zugleich eine Methode des Schutzes gegen Röntgenverbrennungen. *Fortschritte Auf Dem Gebiete Der Roentgenstrahlen*. (14), 27–29.

Laissue, J. A., Blattmann, H., Wagner, H. P., Grotzer, M. A., & Slatkin, D. N. (2007). Prospects for microbeam radiation therapy of brain tumours in children to reduce neurological sequelae. *Developmental Medicine and Child Neurology*, *49*(8), 577–581. https://doi.org/10.1111/j.1469-8749.2007.00577.x

MarkFilipak (2012). Comparison of dose profiles for proton v. x-ray radiotherapy. Retrieved from https://en.wikipedia.org/wiki/Proton_therapy#/media/File:Comparison_of_dose_profiles_for_proton_v._x-ray_radiotherapy.png

Meyer, J., Eley, J., Schmid, T. E., Combs, S. E., Dendale, R., & Prezado, Y. [Yolanda] (2019). Spatially fractionated proton minibeams. *The British Journal of Radiology*, *92*(1095), 20180466. https://doi.org/10.1259/bjr.20180466

Narang, H., Bhat, N., Gupta, S. K., Santra, S., Choudhary, R. K., Kailash, S., & Krishna, M. (2009). Differential activation of mitogen-activated protein kinases following high and low LET radiation in murine macrophage cell line. *Molecular and Cellular Biochemistry*, *324*(1-2), 85–91. https://doi.org/10.1007/s11010-008-9987-y

Ogata, T., Teshima, T., Kagawa, K., Hishikawa, Y., Takahashi, Y., Kawaguchi, A., Suzumoto, Y., Nojima, K., Furusawa, Y., & Matsuura, N. (2005). Particle irradiation suppresses metastatic potential of cancer cells. *Cancer Research*, *65*(1), 113–120.

Paganetti, H., Niemierko, A., Ancukiewicz, M., Gerweck, L. E., Goitein, M., Loeffler, J. S., & Suit, H. D. (2002). Relative biological effectiveness (RBE) values for proton beam therapy. *International Journal of Radiation Oncology*Biology*Physics*, *53*(2), 407–421. https://doi.org/10.1016/S0360-3016(02)02754-2

Particle Therapy Co-Operative Group (2019). Statistics of patients treated in particle therapy facilities worldwide. Retrieved from https://www.ptcog.ch/index.php/patient-statistics. Last accessed on 25/09/2019 at 20:37.

Particle Therapy Co-Operative Group (2019). Particle therapy facilities in clinical operation. Retrieved from https://www.ptcog.ch/index.php/facilities-in-operation. Last accessed on 25/09/2019 at 20:37.

Pawlicki, T., Scanderbeg, D. J., & Starkschall, G. (2016). Physics of Proton Radiation Therapy, in *Hendee's Radiation Therapy Physics*, Fourth Edition, John Wiley & Sons, Inc., Hoboken, NJ, USA. doi: 10.1002/9781118575338.

Peucelle, C., Nauraye, C. [C.], Patriarca, A. [A.], Hierso, E., Fournier-Bidoz, N., Martínez-Rovira, I., & Prezado, Y. [Y.] (2015). Proton minibeam radiation therapy: Experimental dosimetry evaluation. *Medical Physics*, *42*(12), 7108–7113. https://doi.org/10.1118/1.4935868

Prezado, Y. [Y.], & Fois, G. R. (2013). Proton-minibeam radiation therapy: A proof of concept. *Medical Physics*, *40*(3), 31712. https://doi.org/10.1118/1.4791648

Prezado, Y. [Yolanda], Jouvion, G., Guardiola, C., Gonzalez, W., Juchaux, M., Bergs, J., Nauraye, C. [Catherine], Labiod, D., Marzi, L. de, Pouzoulet, F., Patriarca, A. [Annalisa], & Dendale, R. (2019). Tumor Control in RG2 Glioma-Bearing Rats: A Comparison Between Proton Minibeam Therapy and Standard Proton Therapy. *International Journal of Radiation Oncology, Biology, Physics*, *104*(2), 266–271. https://doi.org/10.1016/j.ijrobp.2019.01.080

Prezado, Y. [Yolanda], Jouvion, G., Hardy, D., Patriarca, A. [Annalisa], Nauraye, C. [Catherine], Bergs, J., González, W., Guardiola, C., Juchaux, M., Labiod, D., Dendale, R., Jourdain, L. [Laurène], Sebrie, C., & Pouzoulet, F. (2017). Proton minibeam radiation therapy spares normal rat brain: Long-Term Clinical, Radiological and Histopathological Analysis. *Scientific Reports*, *7*(1), 14403. https://doi.org/10.1038/s41598-017-14786-y

Prezado, Y. [Yolanda], Jouvion, G., Patriarca, A. [Annalisa], Nauraye, C. [Catherine], Guardiola, C., Juchaux, M., Lamirault, C., Labiod, D., Jourdain, L. [Laurene], Sebrie, C., Dendale, R., Gonzalez, W., & Pouzoulet, F. (2018). Proton minibeam radiation therapy widens the therapeutic index for high-grade gliomas. *Scientific Reports*, *8*(1), 16479. https://doi.org/10.1038/s41598-018-34796-8

Raju, M. R. (1995). Proton Radiobiology, Radiosurgery and Radiotherapy. *International Journal of Radiation Biology*, *67*(3), 237–259. https://doi.org/10.1080/09553009514550301

Romanelli, P., Fardone, E., Battaglia, G., Bräuer-Krisch, E. [Elke], Prezado, Y. [Yolanda], Requardt, H. [Herwig], Le Duc, G. [Geraldine], Nemoz, C., Anschel, D. J., Spiga, J., & Bravin, A. [Alberto] (2013). Synchrotron-generated microbeam sensorimotor cortex transections induce seizure control without disruption of neurological functions. *PloS One*, *8*(1), e53549. https://doi.org/10.1371/journal.pone.0053549

Ryan, J. L. (2012). Ionizing radiation: The good, the bad, and the ugly. *The Journal of Investigative Dermatology*, *132*(3 Pt 2), 985–993. https://doi.org/10.1038/jid.2011.411

Sammer, M., Greubel, C., Girst, S., & Dollinger, G. [Günther] (2017). Optimization of beam arrangements in proton minibeam radiotherapy by cell survival simulations. *Medical Physics*, *44*(11), 6096–6104. https://doi.org/10.1002/mp.12566

Sammer, M., Zahnbrecher, E., Dobiasch, S., Girst, S., Greubel, C., Ilicic, K., Reindl, J., Schwarz, B., Siebenwirth, C., Walsh, D. W. M., Combs, S. E., Dollinger, G. [Günther], & Schmid, T. E. (2019). Proton pencil minibeam irradiation of an in-vivo mouse ear model spares healthy tissue dependent on beam size. *PloS One*, *14*(11), e0224873. https://doi.org/10.1371/journal.pone.0224873

Schulz-Ertner, D., & Debus, J. (2013). Hadronentherapie. In Wannenmacher M., Wenz F., Debus J. (Ed.), *Strahlentherapie* (2nd ed., pp. 207–224). Berlin: Springer.

Seegenschmiedt, M. H. (2013). Nebenwirkungen. In Wannenmacher M., Wenz F., Debus J. (Ed.), *Strahlentherapie* (2nd ed.). Berlin: Springer.

Serduc, R., Bräuer-Krisch, E. [Elke], Siegbahn, E. A., Bouchet, A., Pouyatos, B., Carron, R., Pannetier, N., Renaud, L., Berruyer, G., Nemoz, C., Brochard, T. [Thierry], Rémy, C., Barbier, E. L., Bravin, A. [Alberto], Le Duc, G. [Géraldine], Depaulis, A., Estève, F., & Laissue, J. A. (2010). High-precision radiosurgical dose delivery by interlaced microbeam arrays of high-flux low-energy synchrotron X-rays. *PloS One*, *5*(2), e9028. https://doi.org/10.1371/journal.pone.0009028

Serduc, R., Christen, T., Laissue, J., Farion, R., Bouchet, A., van der Sanden, B., Segebarth, C., Bräuer-Krisch, E. [Elke], Le Duc, G. [Géraldine], Bravin, A. [Alberto], Rémy, C., & Barbier, E. L. (2008). Brain tumor vessel response to synchrotron microbeam radiation therapy: A short-term in vivo study. *Physics in Medicine and Biology*, *53*(13), 3609–3622. https://doi.org/10.1088/0031-9155/53/13/015

Trott, K. R. (2010). Second cancer after radiotherapy. In M. C. Joiner & van der Kogel, A. J. (Eds.), *Basic clinical radiobiology* (4th ed., pp. 339–352). London: Hodder Arnold.

Trott, K.-R. [Klaus-Rüdiger] (2017). Special radiobiological features of second cancer risk after particle radiotherapy. *Physica Medica : PM : An International Journal Devoted to the Applications of Physics to Medicine and Biology : Official Journal of the Italian Association of Biomedical Physics (AIFB)*, *42*, 221–227. https://doi.org/10.1016/j.ejmp.2017.05.002

Wannenmacher M., Debus J., Wenz F., Bahnsen J. (2013). Allgemeine Grundlagen. In Wannenmacher M., Wenz F., Debus J. (Ed.), *Strahlentherapie* (2nd ed., pp. 3–10). Berlin: Springer.

Weber KJ., W. F. (2013). Strahlenbiologische Grundlagen. In Wannenmacher M., Wenz F., Debus J. (Ed.), *Strahlentherapie* (2nd ed., pp. 47–85). Berlin: Springer.

WHO/G. Reboux (2018). Fact Sheet on Cancer. Retrieved from https://www.who.int/news-room/fact-sheets/detail/cancer on 10/06/2019 at 10:59

Wilson, R. R. (1946). Radiological use of fast protons. *Radiology*, *47*(5), 487–491. https://doi.org/10.1148/47.5.487

Withers, H. R., Taylor, J. M., & Maciejewski, B. (1988). Treatment volume and tissue tolerance. *International Journal of Radiation Oncology, Biology, Physics*, *14*(4), 751–759.

Wouters, B. G. (2010). Cell death after irradiation: how, when and why cells die. In M. C. Joiner & van der Kogel, A. J. (Eds.), *Basic clinical radiobiology* (4th ed.). London: Hodder Arnold.

Wouters, B. G., & Begg, A. C. (2010). Irradiation-induced damage and the DNA damage response. In M. C. Joiner & van der Kogel, A. J. (Eds.), *Basic clinical radiobiology* (4th ed.). London: Hodder Arnold.

Zabel-du Bois A., Debus J. (2013). Methodik und Technik der stereotaktischen Radiochirurgie. In Wannenmacher M., Wenz F., Debus J. (Ed.), *Strahlentherapie* (2nd ed., pp. 177–186). Berlin: Springer.

Zips, D. (2010). Tumour growth and response to radiation. In M. C. Joiner & van der Kogel, A. J. (Eds.), *Basic clinical radiobiology* (4th ed.). London: Hodder Arnold.

Zlobinskaya, O., Girst, S., Greubel, C., Hable, V., Siebenwirth, C., Walsh, D. W. M., Multhoff, G., Wilkens, J. J., Schmid, T. E., & Dollinger, G. [Günther] (2013). Reduced side effects by proton microchannel radiotherapy: Study in a human skin model. *Radiation and Environmental Biophysics*, *52*(1), 123–133. https://doi.org/10.1007/s00411-012-0450-9

List of publications

Sammer, M., **Zahnbrecher, E.**, Dobiasch, S., Girst, S., Greubel, C., Ilicic, K., et al. (2019). Proton pencil minibeam irradiation of an *in-vivo* mouse ear model spares healthy tissue dependent on beam size. *PloS One*, *14*(11), e0224873. https://doi.org/10.1371/journal.pone.0224873